Transportation Research Part D 109 (2022) 103354

Contents lists available at ScienceDirect

Transportation Research Part D

journal homepage: www.elsevier.com/locate/trd

Exploring the potential of aggregated traffic models for estimating network-wide emissions

S.F.A. Batista [a,*], Gabriel Tilg [b], Mónica Menéndez [a]

[a] Division of Engineering, New York University Abu Dhabi, Saadiyat Marina District PO Box 129188, Abu Dhabi, United Arab Emirates
[b] Chair of Traffic Engineering and Control, Department of Civil, Geo and Environmental Engineering, Technical University of Munich, Arcisstr. 21, 80333 Munich, Germany

ARTICLE INFO

Keywords:
Estimation of emissions
Aggregated traffic models
Macroscopic Fundamental Diagram
Regional networks
COPERT emission model
Sustainability

ABSTRACT

This paper explores the potential of aggregated traffic models based on the Macroscopic Fundamental Diagram for building a network-wide monitoring system of travel emissions. Such a system consists of two layers. In a bottom layer, an aggregated traffic model predicts the network dynamics. In a top layer, an emission model estimates the total exhaust emissions. This paper discusses how to properly calibrate the aggregated traffic models of the bottom layer, to then estimate the total network emissions. We focus on the calibration of travel distances and the network partition definition. We propose a methodology that utilizes the concept of the detour ratio as a proxy to model real travel distances within the aggregated traffic models. This methodology increases the effectiveness of aggregated traffic models for predicting network-wide emissions in realistic scenarios. We also show that the definition of the network partitioning can significantly influence the total network emissions estimation.

1. Introduction

Road transportation is one of the major sources of pollution in urban networks. A study conducted by TomTom (2019) on 416 European cities showed that the congestion index has increased during the last decade. Another study by INRIX (2016) analyzed several congestion indexes of 129 cities in 19 European countries. They estimated the economic cost of congestion to be 183 million sterling pounds between 2016 and 2025, across 123 cities in 19 countries. Additionally, urban congestion and vehicle emissions have been recognized as the major source of toxic pollutants (Masson-Delmotte et al., 2019). Important emissions are carbon dioxide CO_2 and nitrogen oxides NO_x, which are at the origin of climate change phenomena and public health issues. Real-time monitoring systems can play an important role in mitigating the network-wide emissions of these pollutants. However, this requires the design of such reliable monitoring systems in the first place. To this end, aggregated traffic models based on the Macroscopic Fundamental Diagram (MFD) (Daganzo, 2007; Geroliminis and Daganzo, 2008; Vickrey, 2020) represent a promising tool. They can mimic the network-wide traffic dynamics while being computationally efficient. The application of these traffic models requires the partitioning of the city network into regions (Lopez et al., 2017), where traffic conditions are assumed to be approximately homogeneous, i.e. vehicles travel at the same average speed inside each region. The MFD describes the traffic states in each region at a given time interval, relating the number of circulating vehicles (or accumulation) in a region and the average circulating flow. Fig. 1 depicts an example of the urban network partitioning to define the regional network where exchange flows between neighboring regions reflect the aggregated traffic dynamics.

* Corresponding author.
E-mail address: sergio.batista@nyu.edu (S.F.A. Batista).

https://doi.org/10.1016/j.trd.2022.103354

Available online 2 July 2022

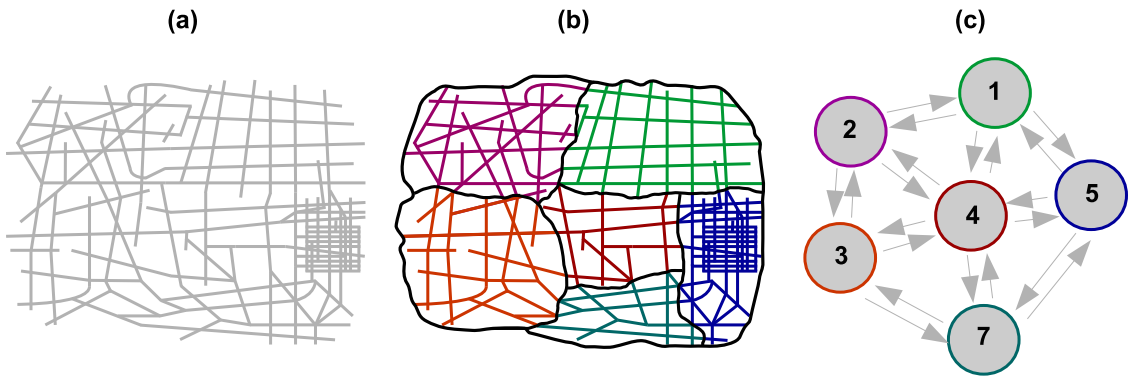

Fig. 1. (a) Urban network. (b) Partitioning of the urban network. (c) Regional network.

The MFD-based traffic models have been successfully used in the literature for a wide range of applications, including optimal control (Sirmatel and Geroliminis, 2019; He et al., 2019; Ren et al., 2020; Kim et al., 2021), route guidance (Yildirimoglu and Geroliminis, 2014; Dandl et al., 2020), pricing schemes (Yang et al., 2019; Loder et al., 2022), incident characterization (Kim and Yeo, 2017; Amini et al., 2020), multimodal transport system design (Dandl et al., 2021; Tilg et al., 2020), and urban parking (Cao and Menendez, 2015). However, the use of these aggregated traffic models for the estimation of network-wide emissions remains an underdeveloped field of research. Shabihkhani and Gonzales (2014) proposed a model that utilizes the MFD relationship to analytically estimate the network-wide emissions from traffic. The model was tested on an idealized ring network, and the estimated emissions were compared to the ones determined by the MOVES emission model (EPA, 2010). Csikós et al. (2015) discussed an optimal control design applied to a traffic network aiming at minimizing network-wide emissions. They utilized the MFD dynamics to mimic traffic conditions in the network. Amirgholy et al. (2017) proposed a model to design a sustainable transit system able to compete with private cars by minimizing the social, economic, and environmental costs of the system. The traffic dynamics were modeled using the MFD. Ingole et al. (2020) proposed an optimal control framework that aims to minimize the total network-wide emissions of urban traffic. They developed a strategy based on a nonlinear model predictive control, and the traffic states in the network were modeled using MFD dynamics. Saedi et al. (2020) proposed a framework to estimate the network-wide emissions combining the MFD to model the traffic dynamics with the microscopic emission model proposed by Panis et al. (2006). Recently, Barmpounakis et al. (2021) established a relationship between the region's speed, accumulation of vehicles, and the total emissions of carbon dioxide CO_2. The authors coined this relationship as the "emissions-MFD". These studies show the potential of the applicability of MFD-based tools for environmental concerns. However, none have analyzed in detail the accuracy of the estimated emissions of pollutants from the MFD-based traffic dynamics. In this paper, we will close that gap.

The main advantage of the MFD-based traffic models is the low computational cost, which enables the development of real-time network-wide monitoring systems of traffic emissions. Such monitoring systems would have two layers: (i) the bottom layer consisting of an MFD-based model that mimics the network dynamics; and (ii) the top layer consisting of an emission model to estimate the network-wide travel emissions based on the MFD dynamics. Before delving into the development of such monitoring systems, it is essential to qualitatively and quantitatively investigate: (a) the accuracy of the aggregated MFD dynamics for estimating the emissions of pollutants; and (b) the proper choice of the emission model considering the aggregated network dynamics. In other words, this requires first to investigate and understand how to properly calibrate an MFD traffic model for reproducing the network dynamics in real-time and consequently discuss the trade-offs on the choice of the emission model. This paper focuses on the first of these two challenges, i.e. how to properly calibrate aggregated MFD traffic models for network-wide estimation of emissions.

The real-time application of the MFD-based models to mimic the network dynamics can be quite complex. To the best of our knowledge, Mariotte et al. (2020) made the first attempt to validate the application of multi-regional MFD-based traffic models using real data. They identified two key elements that play a major role in the modeled network dynamics: (i) the definition of the urban network partitioning; and (ii) the calibration of the travel distances in the regions. The calibration of the travel distances has proven to be a cumbersome task.

To better understand the calibration of travel distances, Fig. 2 shows examples of four trips in the urban network. Focusing on the region highlighted in gray, one can observe that each trip has a different travel distance within this region. This means that at the aggregated level, a journey within this region is characterized by an explicit distribution of travel distances. As depicted in this figure, the calibration of these distributions requires information about a set of trips in the urban network which can be gathered from Global Positioning System (GPS) trajectories of vehicles. Batista et al. (2019) proposed a methodology to determine the explicit distributions of travel distances using a set of trips. Most of the MFD-based applications have considered a single constant average travel distance for all vehicles traveling in the same region. However, this is not representative of all possible travel distances within the region (Batista et al., 2019). Despite this simplistic assumption, in a real implementation of MFD models, one might only have access to a single average travel distance per region. Even when more data is available, there is still uncertainty on Seppecher et al. (2021): (i) the exact real origin and destination of vehicles in the network; (ii) the specific sequence of traveled regions by the individual vehicles; and (iii) the map-matching of the vehicles' trajectories to neighboring links. Moreover, average travel distances

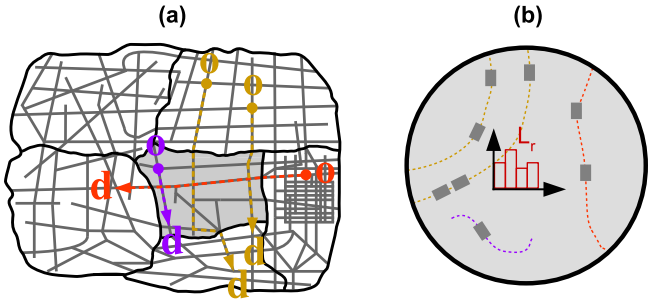

Fig. 2. (a) Example of trips in the urban network. (b) Distribution of travel distances inside the gray region.

also vary in time due to changes in the network dynamics (Yildirimoglu and Geroliminis, 2014; Batista et al., 2021c). In this paper, we discuss an alternative methodology that utilizes the concept of the detour ratio (Yang et al., 2018b) to determine time-varying single average travel distances per region.

Using a simulation-based approach, we propose to qualitatively and quantitatively evaluate how the network partitioning and calibration of travel distances influence the estimation of network-wide emissions of pollutants from traffic dynamics predicted using MFD-based models. We do so by comparing it to a benchmark scenario, that consists of a microscopic traffic simulation using SUMO (Lopez et al., 2018). The whole analysis is performed on the city of Innsbruck, Austria. We utilize the COPERT IV model (Ntziachristos et al., 2009) to determine the network-wide emissions of CO_2 and NO_x. We also showcase the applicability of the proposed methodology to determine time-varying average travel distances for applications of MFD-based models for real-time monitoring of network-wide emissions.

The contributions of this paper are three-fold. First, we propose a methodology to properly calibrate the travel distances using the concept of the detour ratio and a quasi-dynamic approximation. This is important, as we also show that the incorrect calibration of the travel distances can lead to significant discrepancies between the total network exhaust emissions determined based on the MFD dynamics and the benchmark scenario. Second, we show that the definition of network partitioning (i.e. the number of regions, their size, and shape) might influence the total net exhaust emissions. Third, we show that the accumulation-based MFD outperforms the trip-based MFD formulations in terms of accuracy for the estimation of the total network emissions compared to the benchmark scenario. These insights are very important as aggregate traffic models are used more and more often to evaluate traffic emissions and to design strategies to mitigate such emissions.

The remainder of this paper is organized as follows. Section 2 describes the two layers of a network-wide emissions monitoring system that utilizes MFD-based models. We first review the theoretical formulation of the aggregated traffic models based on the MFD and then propose a formulation based on the detour ratio to do a real-time calibration of the average travel distances. Secondly, we review the existing emission models in the literature and describe the dynamics of the COPERT IV model. Section 3 presents the test scenario and describes the settings of the reference scenario. Section 4 presents and discusses the results of the influence of the calibration of the travel distances on the estimation of the network-wide emissions. Section 5 discusses the influence of the network partitioning on the estimation of the network-wide emissions. Section 6 summarizes the conclusions of this paper and discuss future research directions.

2. Real-time monitoring system of network-wide emissions

This section introduces the two components of the network-wide emissions monitoring system. Recall that this monitoring system has two layers. The bottom layer consists of an MFD model that mimics the network dynamics. Section 2.1 introduces the mathematical formulation of MFD-based traffic models and the methodology for estimating time-varying average travel distances. The top layer of the monitoring system consists of an emission model that estimates the emission of pollutants based on the modeled network-wide MFD dynamics. Section 2.2 briefly reviews existing emission models in the literature. This section also provides a detailed description of the COPERT IV model utilized in this paper.

2.1. Bottom layer: Aggregated traffic modeling based on the MFD

The MFD is a generalization of the Fundamental Diagram to a group of neighboring links with similar traffic conditions. It reflects the relationship between the travel production P_r or the spatial mean speed $\overline{v}_r$ and the accumulation n_r of vehicles circulating during a given time interval on a generic region r. Fig. 3 shows an example of the production MFD ($P_r(n_r)$) and the speed MFD ($v_r(n_r)$) functions. In this paper, we assume a bi-parabolic shape for the production MFD, with an inflection point at the critical production P_c and critical accumulation n_c. The critical speed v_c is obtained from the ratio between P_c and n_c. Note that it is possible to convert a speed MFD into a production MFD and vice-versa, as the travel production $P_r(n_r)$ is related to the spatial mean speed $\overline{v}_r(n_r)$ as follows:

$$v_r(n_r) = \frac{P_r(n_r)}{n_r}, \forall r \in X \tag{1}$$

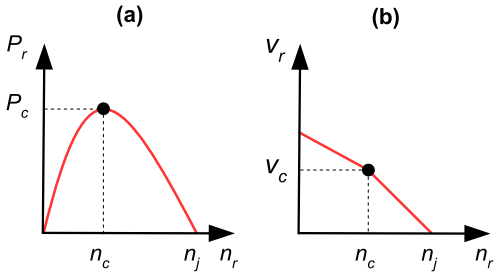

Fig. 3. (a) Production MFD. (b) Speed MFD.

where X is the set of regions defining the regional network.

The accumulation n_r is the sum of all paths' accumulations n_{rp} traveling in region r:

$$n_r = \sum_{r \in X} n_{rp} \cdot \delta_{rp} \tag{2}$$

where δ_{rp} is a binary variable that equals 1 if path p travels on region r, and 0 otherwise. The maximum possible accumulation, n_j, is called the jam accumulation (see Fig. 3).

A path on a regional network represents an ordered sequence of traveled regions from the origin to the destination (Batista et al., 2021b). The path is internal if the travel only occurs inside a single region or regional if multiple regions are crossed. Exchange flows between adjacent regions of vehicles traveling on these paths reflect the traffic dynamics in this kind of aggregated model. The evolution of the vehicles' accumulation traveling on path p and region r, $n_{rp}(t)$, depends on the balance between the cumulative vehicles' inflow $Q_{in,rp}(t)$ and outflow $Q_{out,rp}(t)$:

$$\frac{dn_{rp}}{dt} = Q_{in,rp}(t) - Q_{out,rp}(t), \forall t > 0 \tag{3}$$

Depending on the assumptions made on the outflow function $Q_{out,rp}(t)$, one can distinguish between accumulation-based and trip-based MFD models. Our implementation of these models follows Mariotte et al. (2017) and Mariotte and Leclercq (2019). This refers to the mathematical formulations on how to calculate the inflow $Q_{in,rp}(t)$ and outflow $Q_{out,rp}(t)$ functions for both the trip- and accumulation-based MFD models. The next two subsections introduce these mathematical formulations for general regional networks.

2.1.1. Accumulation-based MFD model

This section introduces the inflow $Q_{in,rp}(t)$ and outflow $Q_{out,rp}(t)$ functions for the accumulation-based model (Mariotte and Leclercq, 2019). Let r_- be the previous traveled region of path p and adjacent to r, and r_+ be the next region to be traveled.

In order to define the inflow and outflow functions, we need to distinguish between internal and regional paths. We start by the definition of the outflow function $Q_{out,rp}(t)$. For an internal path, the outflow function $Q_{out,rp}(t)$ equals the trip completion rate $G_p(n_{rp}(t), n_r(t))$. In the case of a generic region r of a regional path p, the competition between the exit demand function $O_p(n_{rp}(t), n_r(t))$ and the entry supply function $I_p(n_{r_+p}(t), n_{r_+}(t))$ of the next region to be traveled defines the outflow $Q_{out,rp}(t)$. The outflow function $Q_{out,rp}(t)$ then becomes:

$$Q_{out,rp}(t) = \begin{cases} \min(O_p(n_{rp}(t), n_r(t)), I_p(n_{r_+p}(t), n_{r_+}(t))) & \text{if } |p| > 1 \\ G_p(n_{rp}(t), n_r(t)) & \text{if } |p| = 1, \end{cases} \forall r \in X \tag{4}$$

The trip completion rate of an internal path is $G_p(n_{rp}(t), n_r(t)) = \frac{n_{rp}}{n_r} \cdot \frac{P_r(n_r)}{\overline{L}_{rp}}$ (Mariotte and Leclercq, 2019), where $\overline{L}_{rp}$ is the average travel distance of path p in region r.

The exit demand function $O_p(n_{rp}, n_r)$ of a regional path is:

$$O_p(n_{rp}, n_r) = \delta_{rp} \cdot \begin{cases} \frac{n_{rp}}{n_r} \cdot \frac{P_r(n_r)}{\overline{L}_{rp}} & \text{if } n_r < n_c, \\ \frac{n_{rp}}{n_r} \cdot \frac{P_c}{\overline{L}_{rp}} & \text{otherwise.} \end{cases} \tag{5}$$

where δ_{rp} is a binary variable that equals 1 if path p travels in region r, and 0 otherwise.

The entry supply function $I_p(n_{r_+p}(t), n_{r_+}(t))$ of a regional path is:

$$I_p(n_{r_+p}(t), n_{r_+}(t)) = \alpha \cdot \delta_{rp} \cdot \begin{cases} \frac{n_{r_+p}}{n_{r_+}} \frac{P_c}{\overline{L}_{rp}} & \text{if } n_{r_+} < n_c, \\ \frac{n_{r_+p}}{n_{r_+}} \frac{P_{r_+}(n_{r_+})}{\overline{L}_{rp}} & \text{otherwise,} \end{cases} \tag{6}$$

where α is a scaling factor (Mariotte and Leclercq, 2019) to be set larger than 1. This scaling factor ensures that the supply function is not too restrictive.

We now describe the inflow function $Q_{in,rp}(t)$. For an internal path, the inflow function $Q_{in,rp}(t)$ equals the path demand $\Lambda_p(t)$. In the case of a generic region r of a regional path p, the inflow function $Q_{in,rp}(t)$ is simply the competition between the exit demand function of the previous traveled region $O_p(n_{r\_p}(t), n_{r\_}(t))$ and the inflow function of region r, $I_p(n_{rp}(t), n_r(t))$. The inflow $Q_{in,rp}(t)$ is then:

$$Q_{in,rp}(t) = \begin{cases} \min(O_p(n_{r\_p}(t), n_{r\_}(t)), I_p(n_{rp}(t), n_r(t))) & \text{if } |p| > 1 \\ \Lambda_p(t) & \text{if } |p| = 1, \end{cases} \forall r \in X \tag{7}$$

where $O_p(n_{r\_p}(t), n_{r\_}(t))$ and $I_p(n_{rp}(t), n_r(t))$ follow the same rational as in Eqs. (5) and (6), respectively.

2.1.2. Trip-based MFD model

Based on the trip-based formulation introduced by Arnott (2013), the MFD dynamics are centered on the individual distances l_{rp} of each vehicle traveling on path p and region r:

$$l_{rp} = \int_{t_{entry}}^{t_{exit}} v_r(n_r(s))ds \tag{8}$$

where t_{entry} and t_{exit} represent the entry and exit times of a vehicle in a region r; and $v_r(n_r(s))$ is the speed MFD. Note that in the trip-based model one can define as many paths as vehicles, therefore assigning one value of l_{rp} per vehicle. Alternatively, one can also consider a similar average travel distance for all vehicles traveling on the same path p and inside region r, i.e. $\overline{L}_{rp}$.

Based on Eq. (8), Mariotte et al. (2017) derived the outflow function $Q_{out,r}(t)$ for this model:

$$Q_{out,r}(t) = Q_{in,r}(t - T(t)) \frac{v_r(n_r(t))}{v_r(n_r(t - T(t)))} \tag{9}$$

where $T(t)$ is the travel time of the vehicle in region r.

Replacing Eq. (9) into Eq. (3) leads to a system of first-order differential equations with endogenous delay. Solving this system of differential equations requires knowledge about the future state of the system, which is infeasible. Mariotte et al. (2017) and Mariotte and Leclercq (2019) proposed an alternative solution based on an event-based scheme. They assumed a FIFO discipline of all vehicles traveling on the same path p. The first vehicle traveling on path p to enter region r is also the first to complete its trip within this region. The idea behind the event-based scheme is to keep track of the individual position of each vehicle within each region and work with the entry and exit times of all regions. The entry and exit times regulate the order of events in the network, i.e. when a vehicle enters or exits one region. Once a vehicle completes its trip in the region and is allowed to exit, the region's accumulation n_r decreases by one vehicle. On the contrary, when a vehicle enters a region r, the accumulation increases by one vehicle.

We start by introducing the entry time of vehicles within a region r. Let $t^{j-1}_{entry,rp}$ be the entry time of a vehicle $j-1$ traveling on path p and entering region r. Here, we have to distinguish between Origin regions from regional paths, and Intermediate and Destination regions. We also note that we follow the same notation utilized in the previous section, where $r\_$ is the previous traveled region to r. In the case of internal paths or Origin regions, the entry time is $t^{j}_{entry,rp} = t^{j-1}_{entry,rp} + \frac{1}{\Lambda_p(t)}, \forall r \in X$. For Intermediate and Destination regions of regional paths, the entry time is $t^{j}_{entry,rp} = t^{j}_{exit,r\_p}$ where t^{j}_{exit,r_p} is the exit time of the jth vehicle from the previous adjacent region $r\_$.

We now define the exit travel times of region r. We consider the decreasing exit demand function described by Mariotte and Leclercq (2019) for determining the exit times of vehicles from region r. The exit time $t^{j}_{exit,rp}$ of vehicle j from region r is $t^{j}_{exit,rp} = t + \frac{(\overline{L}_{rp} - \overline{L}^{*}(t))}{v_r(n_r)}, \forall r \in X$, where t is the simulation time instant; $\overline{L}^{*}(t)$ is the distance already traveled in region r at t. Note that, in this paper, we consider that all demand is always allowed to enter the region or exit the region when the trips are completed, i.e. we do not consider any border restrictions on the supply or the demand as discussed in Mariotte and Leclercq (2019). This is required to be able to compare the MFD-dynamics with the one resulting from the benchmark scenario, as we explain later in the paper.

2.1.3. Calibration of the travel distances

Although travel distances change over time due to the dynamics of the network (Yildirimoglu and Geroliminis, 2014; Batista et al., 2021a), most of the MFD studies assume they remain invariant. Such assumption affects the realism of the modeled network dynamics, which in our case constitutes the bottom layer of the real-time monitoring system of network-wide emissions. To address this, we propose a methodology to estimate time-varying travel distances per region (i.e. $\overline{L}_r(t), \forall r \in X$).

In fact, we compare three approaches for determining average travel distances per region. The first approach consists of determining static average travel distances ($\overline{L}_r$) per region based on a set of trips, which can either be synthetic or come from GPS trajectories. We refer to this approach as *"Static travel distances"*. This is the standard approach utilized in most of the MFD-based applications, as discussed in the introduction. As explained in Batista et al. (2019) this assumption can lead to significant bias in the modeled network traffic dynamics. However, in this paper, we still consider this approach to shed light on how the influence of a bad calibration of the travel distances can lead to significant errors in the estimation of network-wide emissions.

The second approach consists of determining average travel distances per region based on a set of trips, using a quasi-dynamic approach. We refer to this approach as *"Quasi-dynamic travel distances"*. Similarly, one can utilize a set of GPS trajectories including

their departure times, or forecast the drivers' departure times and determine a synthetic set of shortest trips in distance (Qurashi et al., 2020; Batista et al., 2021a). We split the total simulation time T into M periods, each of length δt. We gather all trips starting during each period δt and determine the average travel distances per region $\overline{L}_r$. This enables us to adjust the average travel distance according to the dynamics of the system especially during the congestion period when drivers tend to take detours to avoid pockets of congestion.

The third approach utilizes the concept of the detour ratio (DR) (Yang et al., 2018b; Paipuri and Leclercq, 2020) to calibrate the travel distances of the synthetic set of trips and the quasi-dynamic approximation to determine the average travel distances per region. We refer to this approach as *"Quasi-dynamic travel distances including a detour ratio"*. Fig. 4 summarizes the different steps of the methodological framework of this third approach. It requires as an input: (i) a set of GPS trajectories; and (ii) a set of origin–destination (OD) pairs of travelers and their departure times. The first step consists of calibrating the DR using the set of GPS trajectories. This is represented by the red dashed line box in Fig. 4. The DR measures how much extra distance beyond the shortest path is traveled on average for each OD pair:

$$DR = \frac{\alpha_1}{d_{sp}^2} + \frac{\alpha_2}{d_{sp}} + \alpha_3 \tag{10}$$

where d_{sp} is the travel distance of the shortest path connecting the OD pair; α_1, α_2 and α_3 are regression coefficients to be fitted based on a synthetic set of shortest trips in distance in the city network.

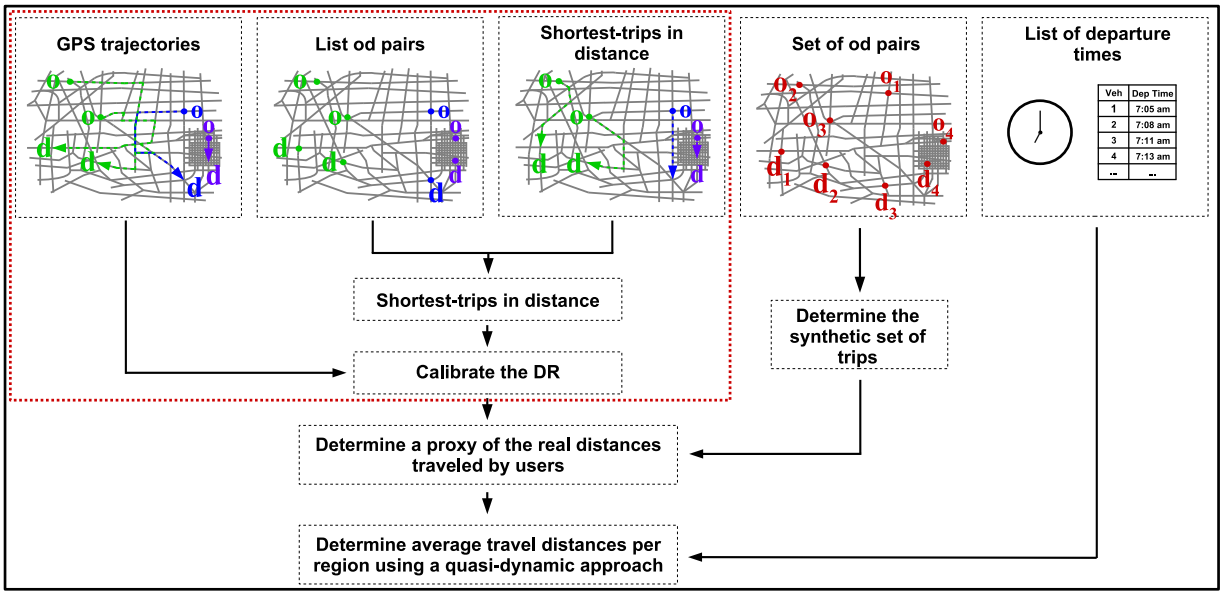

Fig. 4. Methodological framework for estimating average travel distances per region utilizing the concept of the detour ratio. (For interpretation of the references to color in this figure legend, the reader is referred to the web version of this article.)

For each OD pair of the GPS trajectory, we determine the shortest trip in distance. With this information, we then determine the regression coefficients α_1, α_2 and α_3 in Eq. (10). Ideally, the DR changes with the traffic conditions. However, the characterization of time-dependent DR based on empirical data is still an open question in the research literature. In this paper, we follow Yang et al. (2018b) and assume a unique DR, i.e. a unique calibration of the regression coefficients.

The second step consists of calibrating the travel distances of the synthetic set of trips using the DR. We determine the shortest trips in distance for the forecast set of OD pairs. However, drivers do not necessarily choose the route that minimizes their travel distances (Zhu and Levinson, 2015). Therefore, we utilize the calibrated DR as a proxy to determine the real travel distances of drivers and update them on the synthetic set of trips. The third step determines the average travel distances per region using the quasi-dynamic approximation and based on the synthetic set of trips with the updated travel distances. For each δt period, we determine an average travel distance based on all vehicle trips that have departed during this time interval.

2.2. Top layer: Vehicular estimation emissions models

This section describes the top layer of the real-time monitoring system. In this layer, we estimate the network-wide emissions based on the modeled network dynamics. The section starts by providing a brief literature overview of the existing emission estimation models and then describes the formulation of the aggregated emission model COPERT (Ntziachristos et al., 2009) that we utilize in this study.

2.2.1. Review of the estimation emissions models

There are several models discussed in the literature to determine emissions of pollutants related to urban traffic. They can generally be classified into microscopic or macroscopic emissions models (Samaras et al., 2019), depending on their temporal and spatial resolution. They can also be categorized as instantaneous or aggregated emissions models (Fontes et al., 2015). Here, we use the latter classification scheme.

Instantaneous emissions models provide an estimation of emissions and fuel consumption of vehicles at the finest temporal (i.e. 1-s evolution) and spatial scales. Examples of instantaneous emissions models are the CMEM (Barth et al., 2001), MOVES Lite (Frey and Liu, 2013), VT-Micro (Rakha et al., 2004), or PHEM (Hausberger et al., 2009; Luz and Hausberger, 2013). As input data, these models require detailed information about the vehicle kinematics, such as 1-s vehicle-specific speed and acceleration profiles, as well as their trajectories. Such data can readily be obtained from microscopic traffic simulators. However, one should properly calibrate a microscopic traffic model to determine the inputs needed for an instantaneous emissions model (Jie et al., 2013). Both microscopic emissions models and traffic simulators require expensive computations, and their application has been mainly confined to local areas, such as signalized intersections (Madireddy et al., 2011; Sun and Liu, 2015), roundabouts (Quaassdorff et al., 2016), highways (Ahn and Rakha, 2008; Zegeye et al., 2013), or simple theoretical networks (Jamshidnejad et al., 2017). That being said, some scholars have also successfully applied instantaneous emission models to larger networks, such as downtown Los Angeles (USA) (Elbery and Rakha, 2019), the Triangle network that encompasses three American cities (Zhou et al., 2015), the Salt Lake City regional traffic network (Lu et al., 2016), the Buffalo–Niagara metropolitan region's network (Guo et al., 2013), or to downtown Cleveland (USA) (Ahn and Rakha, 2013).

Aggregated emissions models require much less detailed information about vehicle kinematics. More specifically, the necessary inputs include data like the mean speed of a full vehicles' fleet traveling on a region or zone and the total distance traveled. These models are easier to implement for regions such as entire cities up to large metropolitan areas. They have been utilized for the design of control schemes for highways (Pasquale et al., 2017), or to estimate network-wide emissions (Liu et al., 2018). Examples of aggregated emissions models are the EMFAC (CARB, 2007), MOBILE (Environmental protection agency (EPA), 2003), ARTEMIS (Boulter and McCrae, 2007), or the COPERT (Ntziachristos et al., 2009). In this paper, we focus on these aggregated emissions models and, in particular, on the COPERT model.

Two main reasons justify our choice for this emission model. First, we extract highly aggregated traffic variables such as the total travel distances and uniform mean speed profiles for each region from the bottom layer of our system. Both of these variables serve as input data for the COPERT model, ensuring the compatibility between the output data from the MFD-based traffic models and the input data required by the COPERT model. Second, the COPERT model is suitable for determining exhaust emissions for small regions (Lejri et al., 2018; Lejri and Leclercq, 2020). Recall that the application of MFD-based models requires the partition of the urban network into regions that have approximately homogeneous traffic conditions. The next section describes the formulation of the COPERT model.

2.2.2. COPERT model

The COPERT model utilizes unitary emission factors that are a convex function of the region's mean speed $\overline{v}_r, \forall r \in X$. These unitary emission factors are defined for each pollutant y and class of vehicles (i.e. passenger cars, heavy vehicles, trucks, etc.). In this paper, we focus only on passenger cars. For each mean speed value, the unitary emission factors already account for the acceleration and deceleration of vehicles, i.e. driving cycles. The unitary emission factors are calculated based on reference emission data recorded for a mean speed profile using dynamometers installed on a private fleet of vehicles. The data was collected at intervals of 6 min. The fleet composition corresponds to the French urban fleet of 2015, which was, in turn, is obtained from the IFSTTAR fleet updated in 2013. The fleet of passenger cars consists of 30% EURO 5 and 24% Euro 4 diesel vehicles. This follows the works of Lejri et al. (2018) and Lejri and Leclercq (2020). In this paper, we focus on the estimation of the exhaust emissions of carbon dioxide CO_2 and nitrogen oxides NO_x, i.e. $x = \{CO_2, NO_x\}$. We also assume a homogeneous fleet of vehicles in our simulations. This assumption is necessary as the current version of the multi-regional MFD solver (Mariotte et al., 2020) can only handle a single class of vehicles, i.e. it is not able to handle multi-class dynamics.

Ingole et al. (2020) has fitted curves for the recorded unitary emission factors of CO_2 and NO_x using fourth and third-degree polynomial functions, respectively. The regression polynomial for CO_2 is:

$$EF_{CO_2}(\overline{v}_r) = \beta_1 \overline{v}_r^4 + \beta_2 \overline{v}_r^3 + \beta_3 \overline{v}_r^2 + \beta_4 \overline{v}_r + \beta_5 \tag{11}$$

where $\beta_1, \beta_2, \beta_3, \beta_4, \beta_5$ are the regression coefficients, that equal to 4.15×10^{-6}, -1.04×10^{-3}, 1.00×10^{-1}, -4.47 and 123.54, respectively.

The regression polynomial for NO_x is:

$$EF_{NO_x}(\overline{v}_r) = \beta_6 \overline{v}_r^3 + \beta_7 \overline{v}_r^2 + \beta_8 \overline{v}_r + \beta_9 \tag{12}$$

where $\beta_6, \beta_7, \beta_8, \beta_9$ are the regression coefficients, that equal to -6.14×10^{-7}, 2.00×10^{-4}, -2.08×10^{-4} and 9.94×10^{-1}, respectively.

Note that, in this paper, we assume a homogeneous fleet of passenger cars. This means that we apply either Eq. (11) or Eq. (12) to all vehicles to determine the exhaust emissions of CO_2 and NO_x, respectively.

The total emissions ($E_{r,y}, \forall y = \{CO_2, NO_x\}$) are calculated as the product between the unitary emission factors ($EF_y, \forall x = \{CO_2, NO_x\}$) and the total distance traveled by all vehicles in a region r. We approximate the total travel distance by vehicles in region r by the travel production $P_r(n_r)$. We then determine the exhaust emissions $E_{r,y}$, during a given time interval δt, as:

$$E_{r,y} = EF_y(\overline{v}_r) \times P_r(n_r, \overline{v}_r) \times \delta t, \forall r \in X \wedge \forall y = \{CO_2, NO_x\} \tag{13}$$

where n_r is the vehicle accumulation in a region r; and X is the set of all regions defining the regional network. In general, the time interval δt is small (Lejri et al., 2018).

3. Case study and benchmark scenario

This section introduces the test network and the benchmark scenario that consists of a microscopic simulation using SUMO (Lopez et al., 2018). This case study allows us to investigate the suitability of an MFD-based real-time emission monitoring scheme. First, we describe the benchmark model settings including the evaluated demand scenarios. Then, we explain the benchmark model settings for the analysis of the travel distance calibration. Finally, we describe the benchmark model settings examining the effects of different network partition definitions.

3.1. Description of the test scenario

The test network represented in Fig. 5 corresponds to the city of Innsbruck, Austria. The map data was retrieved from OpenStreeMaps (OpenStreetMap contributors, 2020). The network consists of 1992 nodes and 4448 links. We partition this network first into a single region (Fig. 5(a)) and then into four regions (Fig. 5(b)). We consider geographic features of the city network for partitioning into four regions. For example, the Inn river separates regions 2 and 3 from regions 1 and 4, while the main railroad tracks divide regions 1 and 4.

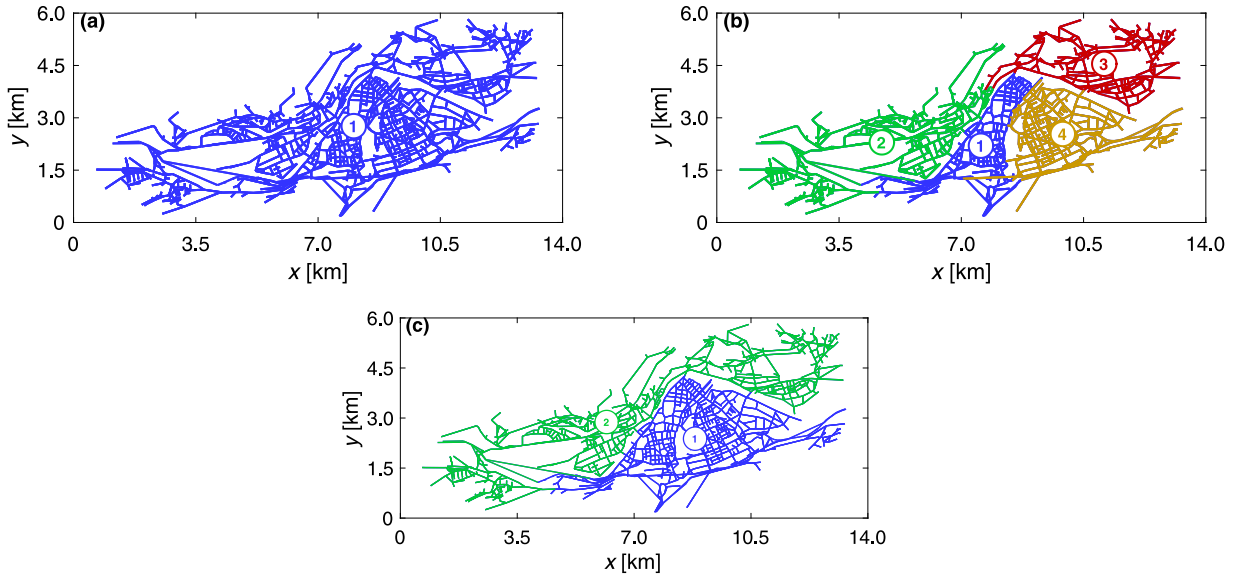

Fig. 5. Innsbruck (Austria) city network. (a) 1-region network. (b) 4-region network. (c) 2-region network. The network data was obtained from OpenStreeMaps (OpenStreetMap contributors, 2020).

We create a benchmark scenario where the traffic dynamics in the city are modeled using the default car-following and lane-changing models in SUMO. We collected the information about the location of traffic signals in the network from OpenStreetMap. This includes 267 junctions in the city network. Unfortunately, the real traffic light settings were not available for this study. For this reason, we assumed that all traffic signals have a common cycle length of 90 s and a green phase of 45 s. We consider three demand scenarios as depicted in Fig. 6, some of which lead to hysteresis loops in the speed MFD functions (Buisson and Ladier, 2009). The demand profiles represent: (i) the loading of the network without the presence of hysteresis on the speed MFD (Fig. 6(a)); (ii) a demand-peak with a substantial hysteresis loop in the speed MFD (Fig. 6(b)); and (iii) a smoother loading and unloading of the network, including a smaller hysteresis loop (Fig. 6(c)).

We refer to these scenarios as demand scenarios 1, 2, and 3 as indicated in Fig. 6. They have a total of 45 833, 15 892, and 34 924 vehicles in the demand scenarios 1, 2, and 3, respectively. We perform the simulations on the full city network of Innsbruck (see Fig. 5(a)) for these three demand scenarios, considering a total simulation time $T = 3.5$ [h]. Drivers are assigned to the shortest paths in time. We consider a quasi-dynamic traffic assignment, where all drivers update their paths en-route considering the perceived traffic dynamics in the network at each interval δt, i.e. all drivers can change en-route the sequence of links to be traveled until they reach their destination if there is an available option with a lower perceived travel time. This kind of assignment represents a reasonable compromise between realism and computational cost (Mühlich et al., 2015). We choose $\delta t = 6$ [min] to be consistent with the period of the recorded reference emission data for calibrating the COPERT model, as described in Section 2.2.2.

Fig. 6(d) to (f) show the speed MFDs resulting from the SUMO microscopic simulations for the full network (Fig. 5(a)) and the three demand scenarios. The circles represent the data points determined from the microscopic simulations. These points are determined using the following procedure. Based on the space–time diagram of the vehicles' trajectories inside region r during δt, we determine the travel production P_r and accumulation n_r as follows:

$$P_r = \frac{1}{T}\sum_{i=1}^{N} td_i\delta_{ir} \tag{14}$$

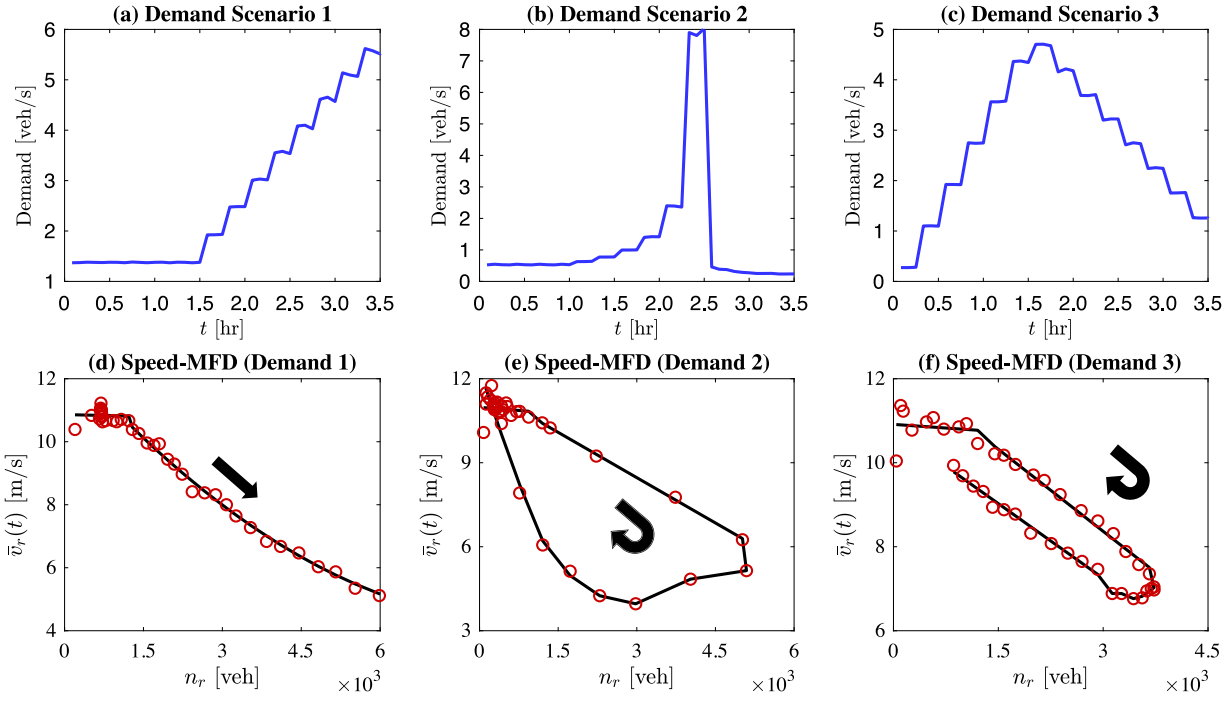

Fig. 6. (a–c) Demand scenarios. (d–f) Speed MFDs of each demand scenario. The red dots represent the values obtained from the SUMO simulation. The black dashed curve represent the fitting of the data points. The black arrows indicate the evolution trend of the speed MFDs.

$$n_r = \frac{1}{T}\sum_{i=1}^{N} tt_i \delta_{ir} \tag{15}$$

where N is the number of vehicles traveling in region r during time interval δt; td_i and tt_i represent the total distance traveled and travel time of vehicle i in region r during δt; and δ_{ir} is a binary variable that equals 1 if vehicle i travels inside region r during δt, and 0 otherwise.

Using Eq. (1), we then determine the mean speed $\bar{v}_r$. Each circle in Fig. 6(d) to (f) represents the mean speed $\bar{v}_r$ and accumulation n_r of vehicles in region r during each time interval δt. We fitted the speed MFDs using a piece-wise linear function of the accumulation n_r (Paipuri et al., 2019). The curves represent the fit to the data points. The black arrows represent the evolution of the mean-speed as a function of the accumulation n_r in the network.

Our goal is to investigate the influence of the calibration of travel distances and the network partitioning on the estimation of the network-wide emissions using the MFD dynamics. However, these variables are highly correlated, and to separately study these effects we need to isolate them both. First, the proper calibration of the travel is necessary as they play a major role in the aggregated traffic dynamics. The MFD assumes homogeneous speeds in the region, which means that all vehicles travel at the same average speed. A longer travel distance can then become a bottleneck as drivers require more time to complete their trips, increasing the accumulation and reducing the mean speed in the region for a longer period. A misrepresentation of travel distances can lead to incorrect estimations of the network dynamics and consequently the estimated emissions. Second, the definition of network partitioning might also introduce a bias on the estimation of the network-wide emissions, as it affects the calibrated travel distances and therefore the traffic dynamics. The two next subsections explain how we determine the emissions for the benchmark scenario using the COPERT model while isolating the effects of the travel distances and the network partitioning. Note that for consistency, we utilize the COPERT model to estimate the network-wide emissions for both the MFD dynamics and the benchmark model.

3.2. Benchmark model settings for investigating the calibration of travel distances

This section describes the methodology implemented to determine the network-wide emissions of the benchmark scenario for the case where we investigate only how the calibration of the travel distances influences the estimation of emissions. This requires disentangling the effects on the estimation of the network-wide emissions resulting from the partitioning and the calibration of the travel distances. For this reason, we fix the partitioning as depicted in Fig. 5, and only change the calibration of the travel distances during these tests. Section 4 presents the detailed analysis.

The question now is how to determine the network-wide emissions based on the reference SUMO simulations for comparison to the ones resulting from the MFD dynamics that utilize different calibration methods of the travel distances (as discussed in

Section 2.1.3). Lejri and Leclercq (2020) showed that emissions are not scale-free, i.e. the estimation of aggregated emissions can lead to significant bias compared to the ones determined based on a more disaggregated level (e.g. road segments). This inconsistency occurs when one utilizes non-scalable variables such as the region's mean speed profiles. As a solution to reduce this inconsistency, Lejri and Leclercq (2020) proposed to use a definition of a distance-weighted speed to determine emissions at the region's level, considering disaggregate information such as the vehicle's travel time and distance within the region. We utilize this approach to determine the regions' emissions based on the SUMO simulations for the testing scenarios discussed in Section 4.

The distance-weighted speed is determined as follows. Consider that there are N vehicles traveling in a region r during a time interval δt. During each interval δt, each vehicle i travels with speed v_i for a travel time tt_i in region r. The spatial mean speed $\overline{v}_r^{ref}$, for each region r and interval δt of the network and for the reference scenario, is determined as (Lejri and Leclercq, 2020):

$$\overline{v}_r^{ref} = \frac{\sum_{i=1}^{N} tt_i v_i}{\sum_{i=1}^{N} tt_i}, \forall r \in X \tag{16}$$

From the SUMO simulations, for each period δt, we determine the travel production (P_r) and accumulation of vehicles (n_r) in each region using Eqs. (14) and (15), and then the spatial mean speed ($\overline{v}_r^{ref}$) using Eq. (16). Considering these variables as inputs, for each period δt, we then determine the total emissions of CO_2 and NO_x utilizing the COPERT model as described in Section 3.2. The total network emissions then result from the sum of the calculated emissions for all periods δt. This procedure is applied for both definitions of the network partitioning depicted in Fig. 5.

3.3. Benchmark model settings for investigating the influence of the network partitioning

This section describes the methodology implemented for determining the network-wide emissions for the benchmark scenario for the test case where we only investigate the influence of the network partitioning. In this case, we determine the travel distances using the "Quasi-dynamic travel distances including a detour ratio" approach. The question is how to define the partitioning to set up as a reference for the benchmark scenario. As previously explained, we need to define an appropriate scale for conducting an environmental assessment using the COPERT model (Lejri and Leclercq, 2020). For this, in this paper, we set two scenarios:

1. The estimation of emissions using the COPERT model is more accurate for smaller regions. For this reason, we investigate how the total network emissions change when the network is partitioned into 1, 2, and 4 regions, as depicted in Fig. 5.
2. For a fixed number of regions, the definition of the network partitioning might also influence the estimation of the network-wide emissions using the COPERT model. For this reason, we also investigate how the total network emissions change when the number of regions is set to 4, but the network partitioning is different. Fig. 7 shows two different types of partitioning for the Innsbruck network.

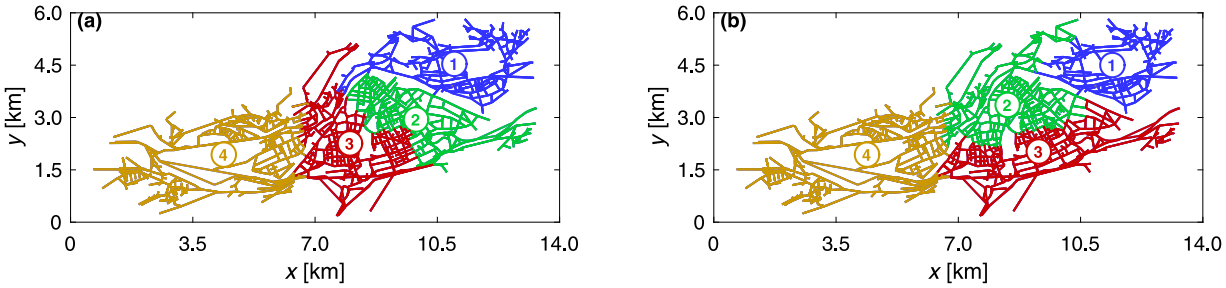

Fig. 7. Different definitions of the network partitioning of Innsbruck considering a fixed number of regions equals to 4.

From the SUMO simulations and for each period δt, we determine the accumulation n_r and spatial mean speed $\overline{v}_r^{ref}$ (using Eq. (16)) for each region. Based on this information, we determine the total emissions of CO_2 and NO_x using the COPERT model. This scenario is set as the reference one to investigate the influence of the network partitioning on the estimation of the network-wide emissions. Section 5 presents the detailed analysis.

4. Calibration of travel distances

This section discusses how the calibration of the travel distances influences the estimation of the network-wide emissions, focusing on the two definitions of the partitioning defined in Fig. 5.

4.1. Whole city of Innsbruck: 1-region

The application of the MFD-traffic models requires the calibration of the distances traveled by vehicles in the regions (Batista et al., 2019). From the benchmark scenario, we gather information about the routes and distances traveled by vehicles in the city network. Following Batista et al. (2021b), these trips represent an internal path in the 1-region network depicted in Fig. 5(a), i.e. they are all internal trajectories within the same region. We utilize the information about the distances traveled by vehicles to characterize the explicit distribution of travel distances of this internal path. The dots in Fig. 8 depict the distance traveled [km] as a function of the departure time [h] of vehicles for the three demand scenarios. The demand peaks happen around 3.5, 2.5, and 1.75 [h] for the demand scenarios 1, 2, and 3, respectively. This is the period when the system is the most congested, explaining the longer travel distances as drivers can change their routes to avoid pockets of congestion.

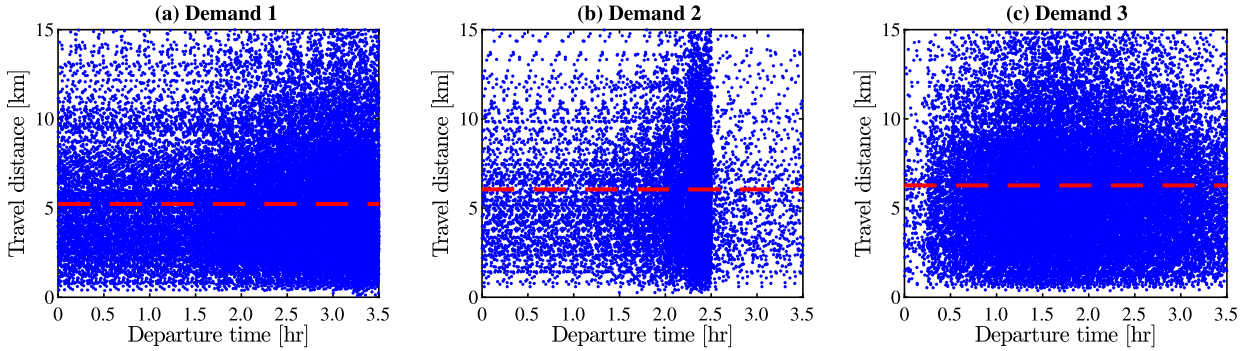

Fig. 8. Distance traveled [km] as a function of the departure time [h] of vehicles represented as blue dots. The horizontal dashed lines represent the average travel distance. The results are depicted for the three demand scenarios.

In the next subsections, we investigate how the network-wide emissions are influenced by the different calibration methods of the travel distances, namely: (i) Static travel distances; (ii) Quasi-dynamic travel distances; and (iii) Quasi-dynamic travel distances including a detour ratio.

4.1.1. Static travel distances

For the calibration of the accumulation- and trip-based MFD models, we consider a static average travel distance $\overline{L}_r$ of 5226 [m], 6045 [m], and 6268 [m] for the demand scenarios 1, 2, and 3, respectively (see the horizontal dashed lines in Fig. 8). Additionally, we consider the setting of the trip-based MFD model using the individual travel distances of vehicles gathered from each of the three demand scenarios. We model the traffic dynamics on the 1-region network (Fig. 5(a)), and determine the emissions of CO_2 and NO_x using the COPERT IV model. Recall that, we determine the network-wide emissions of these two pollutants for the benchmark scenario following the methodology described in Section 3.2. We then calculate the relative differences ϵ between the total emissions ($\sum_{\delta t} E^{MFD}_{r,x}$) determined based on the MFD traffic dynamics and the ones determined from the benchmark SUMO simulation ($\sum_{\delta t} E^{SUMO}_{r,x}$):

$$\epsilon = \frac{\sum_{\delta t} E^{MFD}_{r,x} - \sum_{\delta t} E^{SUMO}_{r,x}}{\sum_{\delta t} E^{SUMO}_{r,x}} \times 100\%, \forall x = \{CO_2, NO_x\} \wedge \forall r \in X \tag{17}$$

Fig. 9 shows the evolution of the accumulation (n_r), mean speeds ($\overline{v}_r$), and outflow ($Q_{out,r}(t)$) as a function of the simulation time t [h] for all three demand profiles. The dashed curves represent the results for the benchmark SUMO simulation. The blue curves show the results for the accumulation-based MFD model. The green and red curves depict the results for the trip-based MFD model calibrated using a static average travel distance and the individual travel distances of vehicles, respectively. Fig. 10 depicts the relative differences ϵ [%] between the emissions of carbon dioxide CO_2 and nitrogen oxides NO_x determined using MFD-based models and the ones determined based on the benchmark SUMO simulation. Again, the results are shown for all three demand scenarios.

One can observe that the trip-based model calibrated with the individual distances traveled by vehicles in the city network provides the closest predictions of the region's accumulation n_r, mean speed $\overline{v}_r$, and outflow $Q_{out}(t)$ to the benchmark SUMO simulation. This naturally leads to low values of the relative error ϵ for the three demand scenarios.

For the demand scenario 1, the accumulation- and trip-based models calibrated using a static *average* travel distance predict a lower accumulation in the region compared to the benchmark SUMO simulation (see Fig. 9(a)). This happens because the average distance traveled (dashed line in Fig. 9(a)) underestimates the distance traveled by several vehicles during the congestion period between ~2 to 3 [h] of the simulation time. As observed in Fig. 9(a), the number of trips with longer travel distances increases during this period because drivers change their paths en-route to others that minimize their travel time, but that has, in general, a longer travel distance. For the MFD-based models, a lower travel distance $\overline{L}_r$ means that drivers complete their trips faster, decreasing the accumulation peak and increasing the mean speed $\overline{v}_r$ concerning the benchmark SUMO simulation. Since the mean speed is higher, the COPERT IV model underestimates the emissions of CO_2 and NO_x as shown in Fig. 10.

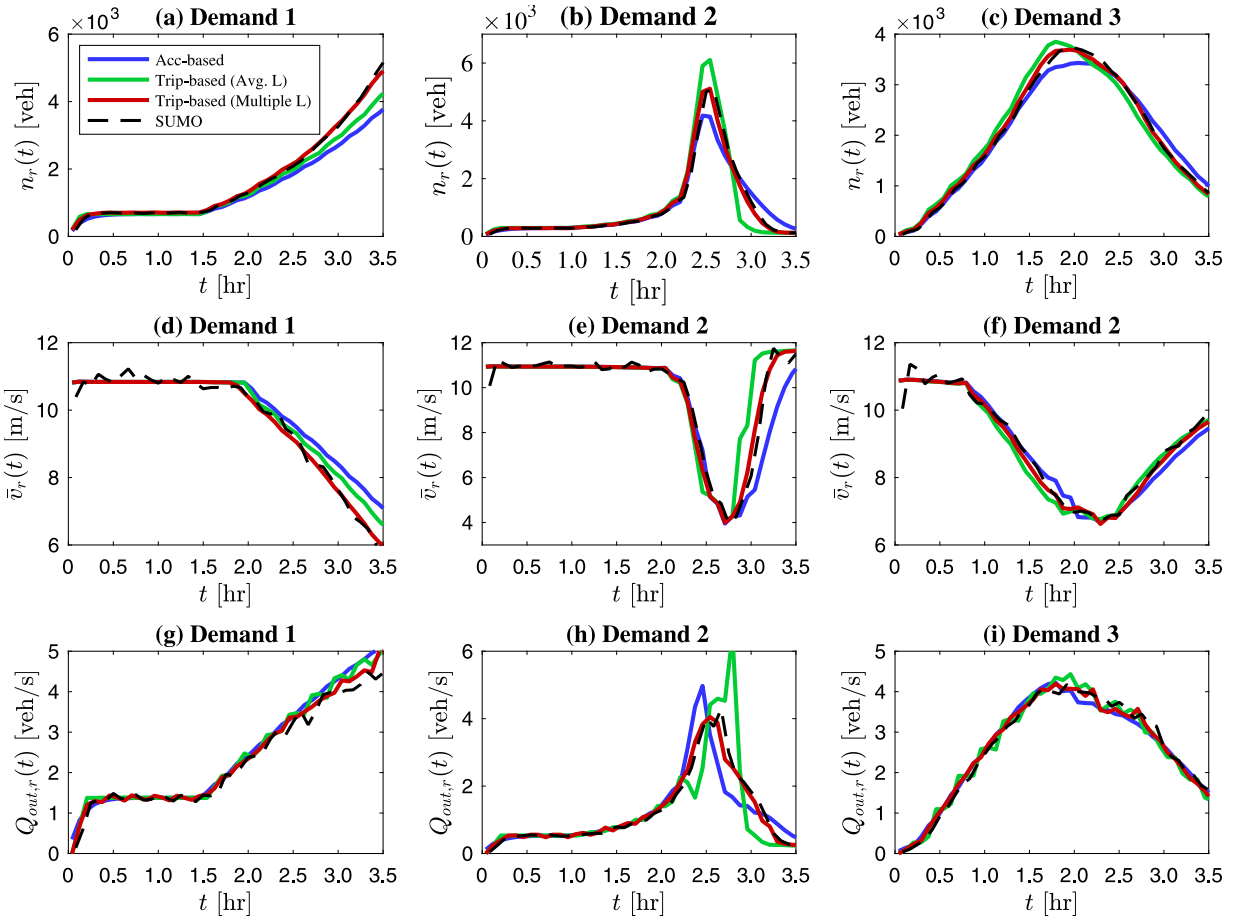

Fig. 9. Evolution of the accumulation n_r [veh], mean speed $\bar{v}_r$ [m/s], and outflow $Q_{out,r}(t)$ [veh/s] as a function of the simulation time t [h]. The black dashed curve represents the results obtained from the SUMO simulation. The blue curve represents the results for the accumulation-based model with an average travel distance. The green and red curves represent the results for the trip-based model calibrated using a single average travel distance and the individual travel distances, respectively. (For interpretation of the references to color in this figure legend, the reader is referred to the web version of this article.)

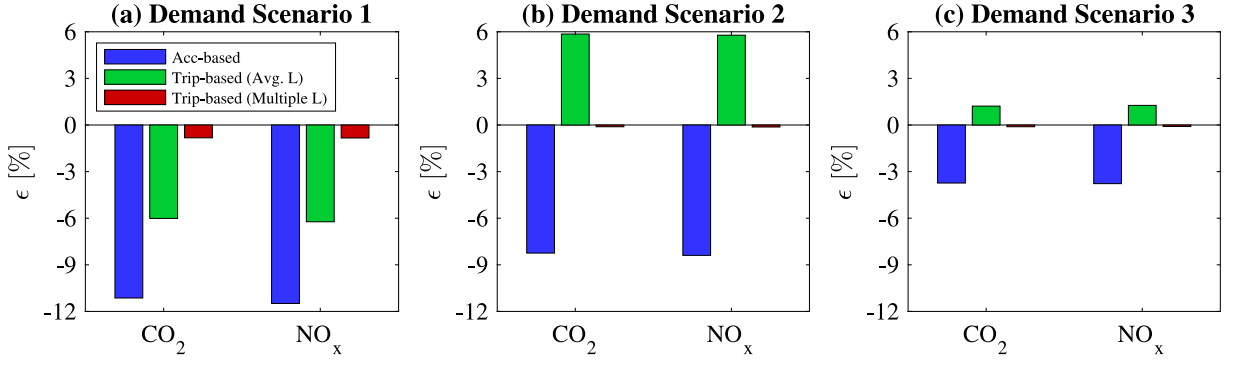

Fig. 10. Relative differences ϵ [%] between the emissions of CO_2 and NO_x estimated using the MFD-based models and the benchmark case for all three demand scenarios.

For the demand scenario 2, a similar trend is also observed around a simulation time of ~2.5 h for the accumulation-based model (see Fig. 9(d) and (e)) compared to the benchmark SUMO simulation. However, during the unloading phase of the region (i.e. around $t \sim 3.0$ h), the static average travel distance is larger than most of the ones of the individual vehicles as observed in Fig. 9(b). This leads to a higher accumulation in the region and a lower mean speed $\bar{v}_r$ than the benchmark SUMO simulation. Overall, the lower accumulation in the region during the congestion peak at ~2.5 [h] has a more significant effect on reducing the

total travel production compared to the benchmark simulation, which leads to an underestimation of the emissions of CO_2 and NO_x as observed in Fig. 10(b). The trip-based MFD model, on the other hand, predicts a higher accumulation and consequently a lower mean speed in the region than the benchmark simulation. This leads to an overestimation of the emissions of CO_2 and NO_x.

In the case of the demand scenario 3, both the trip- and accumulation-based MFD models provide a good estimation of the traffic dynamics (i.e. accumulation n_r and mean speed $\overline{v}_r$) when compared to the benchmark SUMO simulation, as the average travel distance provides a good proxy for the individual traveled distances (see Fig. 8(c)).

4.1.2. Quasi-dynamic travel distances

In this section, we focus on the quasi-dynamic approximation that consists of determining the average travel distance $\overline{L}_r$ at each period of $\delta t = 6$ min. We then apply it within the accumulation-based MFD model and demand scenario 1, as this was the case with the largest relative error ϵ.

Fig. 11 shows the evolution of the accumulation n_r, mean speed $\overline{v}_r$, and outflow $Q_{out,r}(t)$ as a function of the simulation time t, for the accumulation-based MFD model using both the static average travel distance (blue curve) and the quasi-dynamic approximation (dark yellow curve), and the benchmark SUMO simulation (dashed curve). This figure also shows the relative differences ϵ between the CO_2 and NO_x emissions estimated based on the traffic dynamics predicted based on the accumulation-based MFD model compared to the ones determined for the benchmark SUMO simulation. As one can observe, the quasi-dynamic approximation to update the average travel distances improves the prediction of the accumulation and mean speed in the region when compared to the static average travel distance used to calibrate the MFD model. This leads to a reduction of ϵ from $\sim -13\%$ to $\sim -5\%$. This is also observed for the other demand scenarios and the trip-based model (when calibrated with the static average travel distance) however, we do not show it here for brevity.

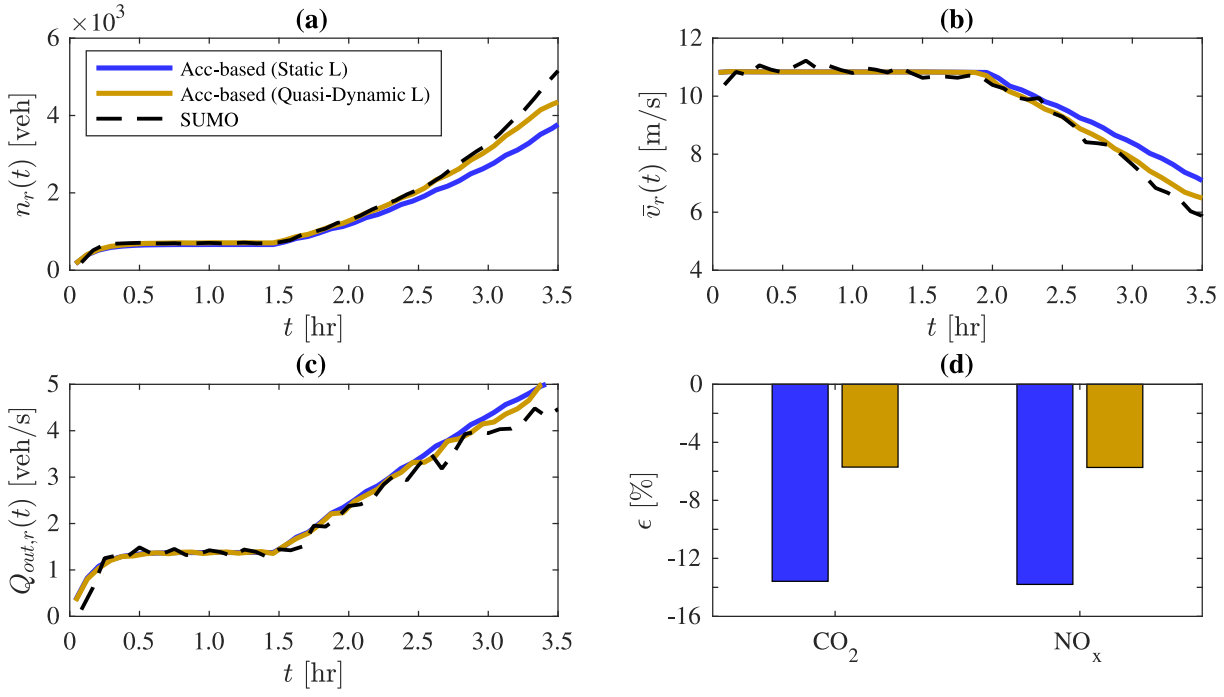

Fig. 11. Evolution of the (a) accumulation n_r [veh]; (b) mean speed $\overline{v}_r$ [m/s]; and (c) outflow $Q_{out,r}(t)$ [veh m/s] as a function of the simulation time t [h]. The black dashed line represents the results gathered from the benchmark SUMO simulation. The blue and green lines represent the results for the accumulation-based model calibrated using a static and quasi-dynamic average travel distance, respectively. (d) Relative differences ϵ [%] between the emissions of CO_2 and NO_x estimated using the two settings of the accumulation-based model and the benchmark from the SUMO simulation. The results depicted refer to the demand scenario 1. (For interpretation of the references to color in this figure legend, the reader is referred to the web version of this article.)

4.1.3. Quasi-dynamic travel distances including a detour ratio

In this section, we showcase the application of the third approach to determining the average travel distances, which utilizes the DR concept. Since we do not have information about the real distribution of the demand in the city of Innsbruck nor a set of GPS trajectories, we focus on the simulation data gathered from the SUMO simulation. We consider the OD pairs of the vehicles' trajectories simulated in SUMO to define the synthetic set η of OD pairs for which we also determine the shortest trips in distance.

We discuss four different calibration methods of the DR (see Eq. (10)). From the first to the fourth cases, we sample a subset of 10% (case 1), 20% (case 2), 50% (case 3), and 100% (case 4), respectively, from the full sets of trajectories (i.e. based on the full SUMO simulation) for all demand scenarios. This enables us to calculate the regression coefficients and then determine a proxy for the actual travel distances. In this paper, we assume a unique DR for all trips, i.e. we only calibrate the regression coefficients once. This assumption is in line with Yang et al. (2018b) and Paipuri and Leclercq (2020).

Fig. 12 shows the relative error ϵ [%] for the four cases and the three demand scenarios. The results are depicted for the accumulation- and trip-based models. The relative errors ϵ [%] are approximately equal and relatively low (i.e. in general less than 5%) for cases 1 to 4, compared to the reference SUMO simulation. This is observed for both MFD models and all three demand scenarios. The relative errors ϵ are consistent for cases 1 to 4, which is a good indicator. As one can also observe, case 1 provides similar relative errors ϵ to case 4. This shows that a small subset corresponding to 10% of the full set of trajectories is already a good proxy to calculate the regression parameters in Eq. (10), and then determine the travel distances.

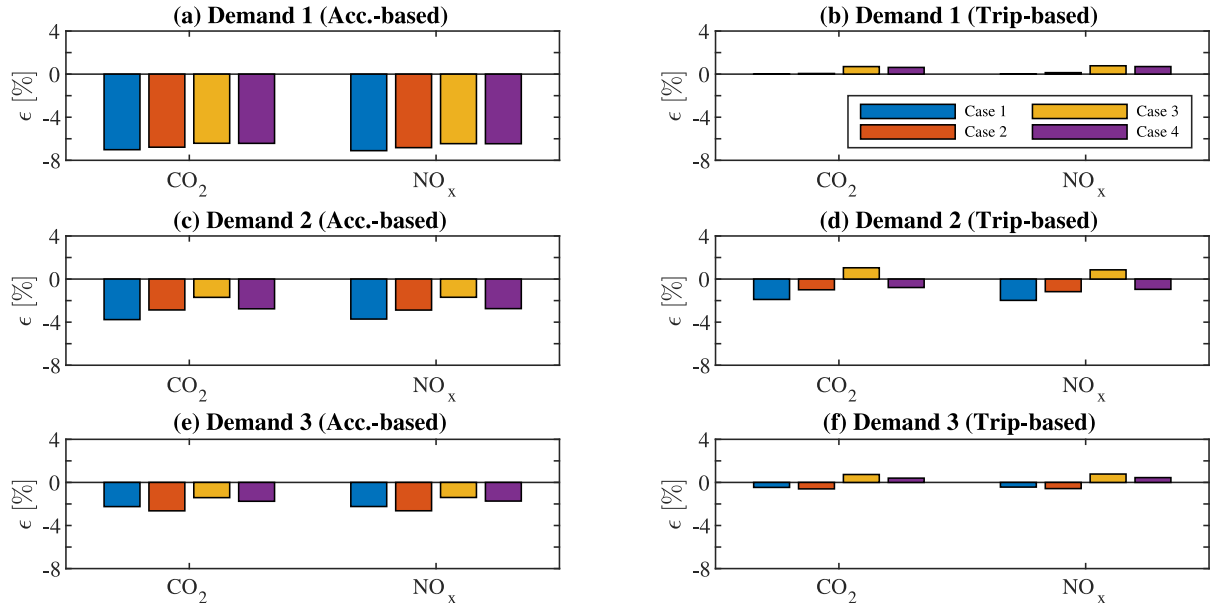

Fig. 12. Relative error ϵ [%] for cases 1 to 4 and all three demand scenarios. The left panels show the results for the accumulation-based model. The right panels show the results for the trip-based model.

4.1.4. Comparative analysis between the different methods to calibrate the travel distances

This section discussed how the calibration of the travel distances influences the estimation of network-wide emissions for the 1-region network.

Since MFD models assume that the mean speed $\overline{v}_r$ is homogeneous in each region r, a lower travel distance means that vehicles can finish their trips faster, increasing the mean speed and decreasing the accumulation in the region. A longer travel distance of a path in a region r might act as a bottleneck, as drivers need more time to complete their trips in the region, increasing the congestion level for longer and reducing the mean speed. This has two important consequences on the estimation of emissions. First, an increase of the mean speed $\overline{v}_r$ leads to a lower emission factor. Second, a lower accumulation of vehicles in the region also leads to a lower travel production. This results in an underestimation of the emissions of CO_2 and NO_x compared to the benchmark SUMO simulation, when using the COPERT IV model. The opposite trend in the region's accumulation n_r and mean speed $\overline{v}_r$, results in an overestimation of the emissions. Therefore, the calibration of travel distances becomes one key element in the calibration of real-time network-wide monitoring systems of travel emissions.

The results discussed in this section clearly show that a static average travel distance is a good proxy to calibrate the accumulation-based MFD model when the distance traveled as a function of the departure time is approximately uniformly distributed over time (e.g. demand scenario 3). However, in realistic scenarios, this travel distance is not necessarily uniformly distributed. Thus, we need better proxies to calibrate the travel distances for the application of MFD models, and ideally, reduce the relative error when estimating the CO_2 and NO_x emissions. In this context, the proposed methodology based on the DR concept and a quasi-static approximation to calibrate the travel distances prove to be an efficient approach. Therefore, hereafter, we focus our analysis on the most promising approach to calibrate the travel distances, i.e. *"Quasi-dynamic travel distances including a detour ratio"*.

4.2. 4-region network

This section investigates how the calibration of the travel distances using the DR and a quasi-dynamic approximation performs in the multi-region context. For this, we consider the Innsbruck network partitioned into four regions as depicted in Fig. 5(b). We model the traffic dynamics in the regions using both the accumulation- and trip-based MFD models and focus on demand scenario 2. We calibrate the speed MFDs based on the output data from SUMO. This scenario represents a demand peak with the presence of hysteresis on all four MFD functions. Additionally, we calibrate the demand for each one of the 16 regional OD pairs based on the benchmark SUMO simulation. Furthermore, we filter the trajectories of vehicles by the sequence of traveled regions to gather the

paths on the regional network. This yields a total of 34 paths. Recall that we determine the network-wide emissions of these two pollutants for the benchmark scenario following the methodology described in Section 3.2. Also note, that we do not consider any entry supply or exit demand restrictions in order to be able to reproduce the traffic dynamics as one of the benchmark scenario. This is because such restrictions were not applied either in the SUMO simulations.

We determine a single average travel distance per region independent of the path traveled by vehicles. This means that vehicles traveling in the same region but on different paths have the same average travel distance. Since we do not have a set of GPS trajectories available for the city of Innsbruck, we randomly select a subset of 10% of the trips from the full set of the trajectories of the vehicles modeled in SUMO for demand scenario 2. We determine the shortest trips in distance connecting the same OD pairs like the ones listed in the subset. With this information, we then determine the regression coefficients in Eq. (10). Similar to the previous section, we assume that the distribution of the demand is given by the OD pairs of the trajectories of the vehicles simulated in SUMO. We then determine the travel distances based on the DR and estimated regression coefficients (see Eq. (10)).

Fig. 13 depicts the evolution of the accumulation $n_r(t)$ [veh] as a function of time t [h] for both the accumulation- (blue curve) and trip-based (green curve) MFD models and the benchmark SUMO simulation (dashed curve). Fig. 14 depicts the relative differences ϵ [%] between the CO_2 and NO_x emissions estimated based on the modeled traffic dynamics by both MFD models and the ones estimated using the benchmark SUMO simulation. As one can observe, both MFD models are able to mimic traffic dynamics in the regions similar to the benchmark model. There are only some small differences between the accumulations predicted by the MFD models and the benchmark SUMO simulation during the loading and unloading phases of each region. These differences occur because the estimated average travel distances per region using the DR tend to be slightly shorter than the ones directly determined from the vehicles' trajectories, using the quasi-dynamic approximation. The relative errors ϵ for the emission estimation in the case of the accumulation-based model are still acceptable. They are slightly larger for some regions, e.g. regions 1 and 3, in the case of the trip-based model.

All in all, predicting the traffic dynamics in a multi-regional network and therefore the network-wide emissions of CO_2 and NO_x is more complex than in a single region network. The methodology based on the DR to calculate the travel distances has proven to be efficient also for these applications.

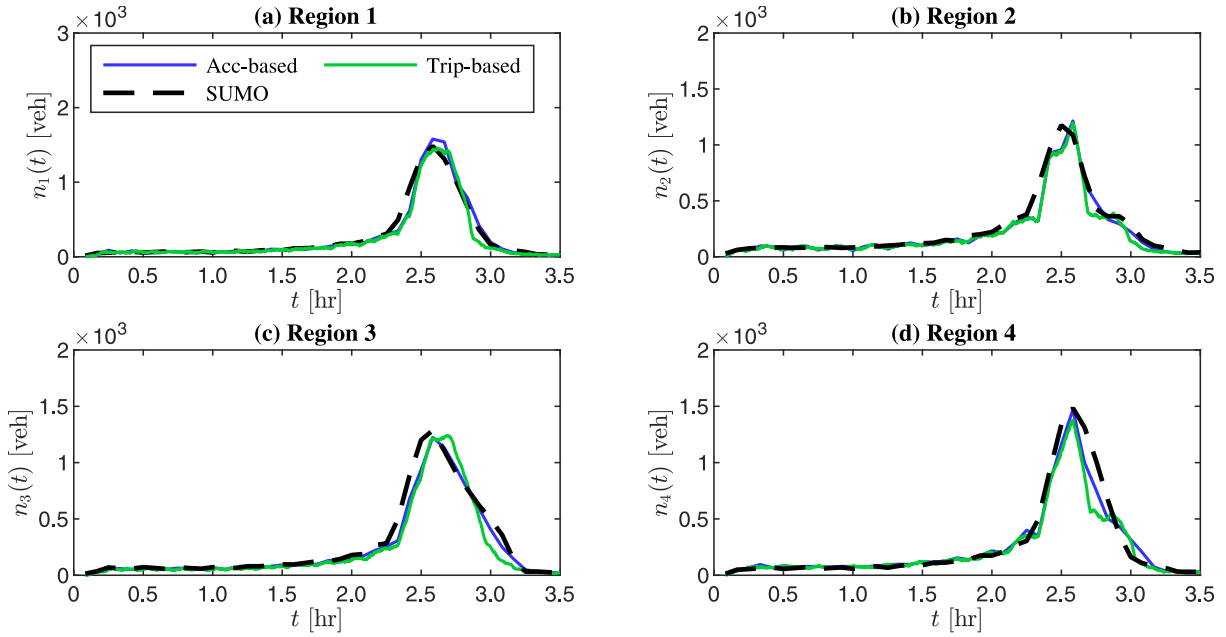

Fig. 13. Evolution of the accumulation $n_r(t)$ [veh] in the regions as a function of time t [h]. The results are depicted for the accumulation-based MFD model (blue curve), trip-based MFD model (green curve) and the benchmark SUMO simulation (black dashed curve). (For interpretation of the references to color in this figure legend, the reader is referred to the web version of this article.)

5. Partitioning of the urban network

This section describes how the definition of the partitioning of the urban network and the number of regions in which the network is partitioned influence the network-wide emissions of carbon dioxide CO_2 and nitrogen oxides NO_x, estimated using the modeled MFD traffic dynamics.

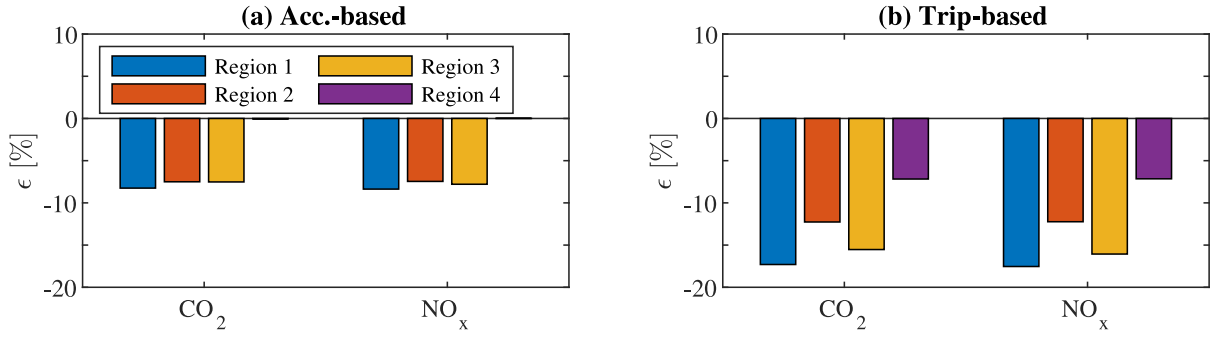

Fig. 14. Relative differences ϵ [%] between the emissions of CO_2 and NO_x estimated using the MFD-based models and the benchmark SUMO simulation.

5.1. Number of regions

Here, we model the MFD dynamics (both accumulation- and trip-based) for the cases of the 1-, 2- and 4-region network as described in Section 3.3, and for all three demand scenarios. We then estimate the network-wide emissions for these scenarios using the COPERT model and the modeled MFD dynamics. We determine the relative differences β between the total emissions ($E_x^{z=1,2}, \forall x = \{CO_2, NO_x\}$) determined based on the MFD traffic dynamics modeled for the 1- and 2-region network and the ones determined from the network partitioned into 4 regions ($E_x^{z=4}, \forall x = \{CO_2, NO_x\}$):

$$\beta = \frac{E_x^{z=1,2} - E_x^4}{E_x^4} \times 100\%, \forall x = \{CO_2, NO_x\} \tag{18}$$

Fig. 15 depicts the relative differences β [%] between the network-wide emissions determined based on the network partitioned into 1 and 2 regions, and the ones determined from the network partitioned into 4 regions. This figure shows the results for all three demand scenarios, and both the accumulation- and trip-based MFD models as well as both pollutants (i.e. CO_2 and NO_x). The blue bars represent the relative differences β between the 1-region partitioning and the 4-region, while the green bars refer to the relative differences β between the 2- and 4-region cases.

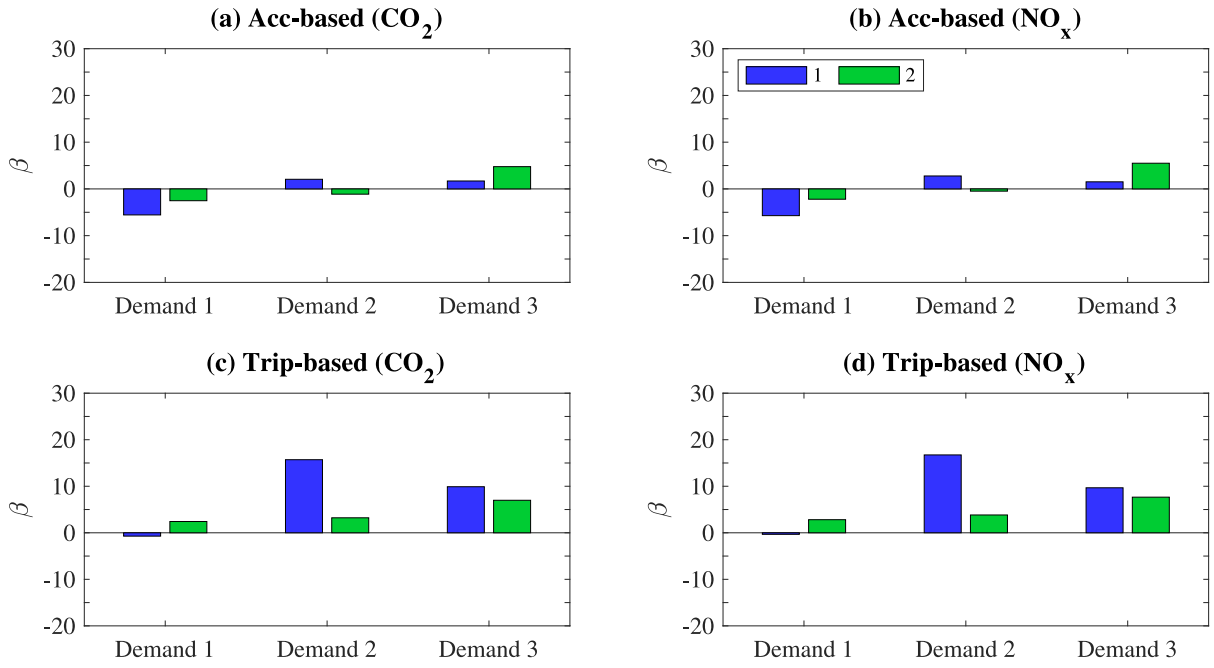

Fig. 15. Relative differences β [%] between the total emissions of carbon dioxide CO_2 and nitrogen oxides NO_x, determined based on the accumulation- and trip-based MFD dynamics for the 1- and 2-region networks, and the 4-region network. The results are depicted for the three demand scenarios. (For interpretation of the references to color in this figure legend, the reader is referred to the web version of this article.)

From Fig. 15, one can observe that as a general result, the estimated network-wide emissions are not only influenced by the number of partitions but also by the travel demand pattern, i.e. how the demand is distributed over the network concerning the definition of the partition. In some cases, the relative differences β decrease as the number of regions also increases. However, this is not observed in other cases. The distribution of the travel demand over the network concerning the definition of the partition plays an important role in the calibration of the average travel distances per region. The average travel distances for the 1- and 2-region network only represent an approximation of the ones of the four regions (Batista et al., 2019), which completely changes the traffic dynamics in the network. Longer travel distances mean that drivers require more time to complete their trips, increasing the level of congestion and therefore travel emissions. The trip-based model also shows, in general, larger relative differences β than the accumulation-based, for Demands 2 and 3. Recall that the core of the trip-based model relies on the travel distances of vehicles. The average travel distance for the full network only represents a rough approximation of the ones of each of the four regions, explaining why we observe the largest relative differences β for demand scenarios 2 and 3 and the 1-region network case. The relative differences are smaller for the 2-region case, as the average travel distances represent a better proxy of the ones of the four regions.

5.2. Definition of the network partitioning for a fixed number of regions

Here, we model the network dynamics using both the accumulation- and trip-based MFD models for the 4-region networks depicted in Figs. 5(b) and 8. Again, we determine the network-wide emissions using the COPERT model for the three demand scenarios. We then calculate the relative differences $\phi_{ij}, \forall(i,j) = 1,2,3 \wedge i \neq j$ between the total emissions determined for the different definitions of the network partitioning:

$$\phi_{ij} = \frac{E_x^i - E_x^j}{E_x^j} \times 100\%, \forall x = \{CO_2, NO_x\} \wedge \forall(i,j) = 1,2,3 \wedge i \neq j \tag{19}$$

Fig. 16 depicts the relative differences ϕ between the total network emissions of CO_2 and NO_x determined based on the accumulation- and trip-based MFD dynamics of partitioning 2 and 1 (ϕ_{12}), Partitioning 3 and 1 (ϕ_{13}), and Partitioning 3 and 2 (ϕ_{23}). The results are depicted for all three demand scenarios.

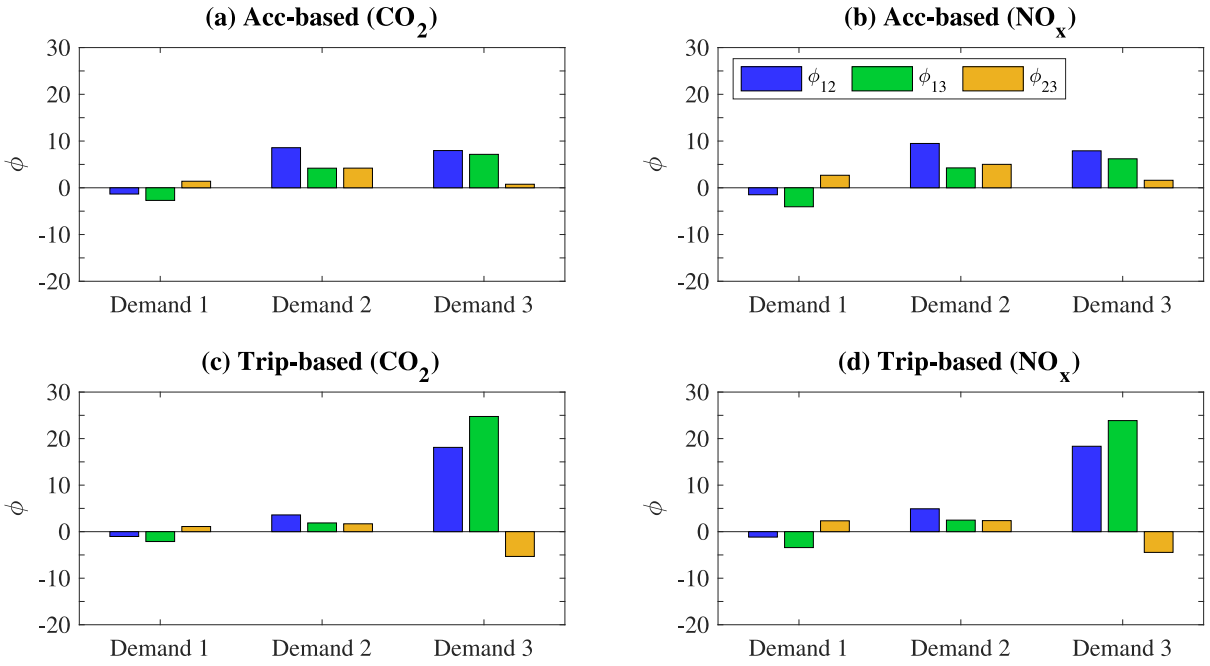

Fig. 16. Relative differences ϕ [%] between the total emissions of carbon dioxide CO_2 and nitrogen oxides NO_x, determined based on the accumulation- and trip-based MFD dynamics for the Partitioning 2 and 3 with respect to Partitioning 1. The results are depicted for the three demand scenarios.

As one can observe, for some demand scenarios, the relative differences ϕ are very close to 0 (e.g. Demand 1). In other scenarios, the relative differences can go up to ~10% or even ~20%. These results clearly show that the definition of the network partitioning can have a significant impact on the estimation of the total emissions of the network. In fact, changing the size and shape of the regions plays a significant role in the modeled MFD dynamics as this can significantly change the calibration of the average travel distances, as also discussed in the previous section. A change in the topological features of a region also changes the spatial distribution of the demand inside this region, and therefore the weights of each individual travel distance on the calculation of the

region's average travel distance (Batista et al., 2019). This is what happens in the case of demand scenario 3 and the trip-based MFD dynamics, when comparing the total network emissions of partitioning 2 and 3 against partitioning 1. On the other hand, increasing the size of a region also increases the level of aggregation required for determining the average travel distance. This results on a larger error in the calculation of the average travel distance (Batista et al., 2019), i.e. the average travel distance might be a rough approximation of the real distances traveled within the region.

6. Discussion and conclusions

This paper analyzes the suitability of MFD-based traffic modeling to build a real-time monitoring system of network-wide emissions. Such a monitoring system is composed of two layers. One layer corresponds to the MFD traffic dynamics modeling. The other layer corresponds to a macroscopic emission model that determines the total network emissions based on the MFD dynamics. This paper puts a strong focus on the first layer. The utilization of the MFD concept enables real-time application due to its low computational cost. We qualitatively and quantitatively investigate how the calibration of average travel distances and the definition of the network partitioning influence the estimation of the network-wide emissions of CO_2 and NO_x. We estimate the total emissions using the COPERT IV emission model. We set up a benchmark scenario that represents the ground truth and consists of a microscopic simulation of the traffic dynamics in SUMO. The city of Innsbruck, used as a test network, is analyzed considering different definitions of the partitioning and number of regions. We studied three different demand profiles corresponding to (i) the network loading without the presence of hysteresis on the MFD; (ii) the network loading and unloading with a large hysteresis loop; and (iii) a smoother demand-peak with the presence of a smaller hysteresis loop.

Our results clearly show the importance of the proper calibration of the travel distances for the modeled MFD dynamics and the resulting total network emissions. For the single-region network, we show that the trip-based MFD model calibrated with individual travel distances can reproduce the traffic dynamics well compared to the benchmark scenario, leading to relative errors $\epsilon \sim 0\%$ on the estimation of the CO_2 and NO_x emissions. However, the relative errors increase when a single static average travel distance is utilized to calibrate both the trip- and accumulation-based MFD models. Alternatively, we propose a methodology that utilizes a set of synthetic trips and the concept of the detour ratio for calibrating average travel distances. We consider a quasi-dynamic approximation where we determine the average travel distances at each time interval δt. This methodology has proven to be effective for the prediction of the traffic dynamics for both the trip- and accumulation-based MFD models on a single-region network. Results from the case study show relative errors typically lower than $\sim 5\%$ on the estimation of the CO_2 and NO_x emissions compared to the benchmark SUMO simulation. The same is true for the 4-region network. However, the relative errors of the trip-based MFD models are slightly larger than the ones of the accumulation-based MFD model. Overall, we conclude that the MFD models are an efficient tool to predict the traffic dynamics and the resulting network-wide emissions, but particular attention should be given to the proper calibration of the travel distances.

We have also investigated the influence of the definition of the number and shape of regions in the network resulting from the partitioning on the estimation of the total network emissions. Based on our experiments, we clearly show that not only does the number of regions, their size and shape influence the estimation of the network emissions, but that it also depends on how the demand is distributed over the network concerning the partitioning which strongly influences the calibration of the travel distances.

This paper opens the door for research on the development of monitoring systems of network-wide emissions considering the MFD traffic dynamics. As the next natural step, we will investigate different aggregated emission models to estimate the total net exhaust emissions based on the MFD dynamics. The accuracy of these models will be analyzed against a more detailed instantaneous emission model. Our results also show that there is a need for future research on the setting of appropriate partitioning criteria for the application of MFD models from the traffic emissions in the multi-region context. We also further note that a more detailed analysis (out of the scope of this paper) could sample many different regions (e.g., 100 different 2-region networks, 100 different 4-region networks, etc.) and compare the results. This, however, would not be aligned with the existing literature on partitioning network for MFD models. In fact, there are very specific and smart ways of doing partitioning, and this process should not be random.

CRediT authorship contribution statement

S.F.A. Batista: Conceptualization, Methodology, Case study design, Validation and results analysis, Writing of the original draft of the paper. **Gabriel Tilg:** Performed the microscopic simulations with SUMO, Participated in the case study design and conceptualization of the paper, Review & editing of the paper. **Mónica Menéndez:** Conceptualization, Methodology, Review & editing of the paper.

Acknowledgments

We thank the reviewers for their comments and suggestions which have much improved the quality of our paper. S. F. A. Batista and M. Menéndez acknowledge support by the NYUAD Center for Interacting Urban Networks (CITIES) and by the NYUAD Arabian Center for Climate and Environmental Sciences (ACCESS), funded by Tamkeen under the NYUAD Research Institute Award CG001 and the NYUAD Research Institute Award CG009, respectively. Gabriel Tilg acknowledges the support by the research project MobiDig: Mobilität Digital Hochfranken funded by the German Federal Ministry of Transport and Digital Infrastructure. S. F. A. Batista thanks Mahendra Paipuri for the discussions and brainstorming about the modeling of the hysteresis effects with Macroscopic Fundamental Diagram based traffic models. All the authors have approved the final version of this paper submitted to publication.

References

Ahn, K., Rakha, H., 2008. The effects of route choice decisions on vehicle energy consumption and emissions. Transp. Res. D 13 (3), 151–167. http://dx.doi.org/10.1016/j.trd.2008.01.005.

Ahn, K., Rakha, H.A., 2013. Network-wide impacts of eco-routing strategies: A large-scale case study. Transp. Res. D 25, 119–130. http://dx.doi.org/10.1016/j.trd.2013.09.006.

Amini, S., Tilg, G., Busch, F., 2020. Macroscopic traffic dynamics in urban networks. In: Proceedings of the 99th Transportation Research Board Annual Meeting (CD-ROM), 12-16 January, Washington, DC, USA.

Amirgholy, M., Shahabi, M., Gao, H.O., 2017. Optimal design of sustainable transit systems in congested urban networks: A macroscopic approach. Transp. Res. E 103, 261–285. http://dx.doi.org/10.1016/j.tre.2017.03.006.

Arnott, R., 2013. A bathtub model of downtown traffic congestion. J. Urban Econ. 76, 110–121. http://dx.doi.org/10.1016/j.jue.2013.01.001.

Barmpounakis, E., MartíMontesinos-Ferrer, Gonzales, E.J., Geroliminis, N., 2021. Empirical investigation of the emission-macroscopic fundamental diagram. Transp. Res. D 101, 103090. http://dx.doi.org/10.1016/j.trd.2021.103090.

Barth, M., Malcom, C., Scora, G., 2001. Integrating a comprehensive modal emissions model into atmis transportation modeling frameworks. URL: https://escholarship.org/uc/item/6248p2dr.

Batista, S.F.A., Ingole, D., Leclercq, L., Menéndez, M., 2021c. The role of trip lengths calibration in model-based perimeter control strategies. IEEE Trans. Intell. Transp. Syst. 1–11. http://dx.doi.org/10.1109/TITS.2021.3049679.

Batista, S.F.A., Leclercq, L., Geroliminis, N., 2019. Estimation of regional trip length distributions for the calibration of the aggregated network traffic models. Transp. Res. B 122, 192–217. http://dx.doi.org/10.1016/j.trb.2019.02.009.

Batista, S., Leclercq, L., Menéndez, M., 2021a. Dynamic traffic assignment for regional networks with traffic-dependent trip lengths and regional paths. Transp. Res. C 127, 103076. http://dx.doi.org/10.1016/j.trc.2021.103076.

Batista, S., Seppecher, M., Leclercq, L., 2021b. Identification and characterizing of the prevailing paths on a urban network for MFD-based applications. Transp. Res. C 127, 102953. http://dx.doi.org/10.1016/j.trc.2020.102953.

Boulter, P.G., McCrae, I.S., 2007. Assessment and reliability of transport emission models and inventory systems (artemis) - final report. URL: https://trl.co.uk/sites/default/files/PPR350.pdf.

Buisson, C., Ladier, C., 2009. Exploring the impact of homogeneity of traffic measurements on the existence of macroscopic fundamental diagrams. Transp. Res. Rec. J. Transp. Res. Board 2124, 127–136. http://dx.doi.org/10.3141/2124-12.

Cao, J., Menendez, M., 2015. System dynamics of urban traffic based on its parking-related-states. Transp. Res. B 81, 718–736. http://dx.doi.org/10.1016/j.trb.2015.07.018, ISTTT 21 for the year 2015.

CARB, 2007. EMFAC2007/version 2.30. User's guide: Calculating emission inventories for vehicles in California. URL: https://ww3.arb.ca.gov/msei/onroad/downloads/docs/user_guide_emfac2007.pdf.

Csikós, A., Tettamanti, T., Varga, I., 2015. Macroscopic modeling and control of emission in urban road traffic networks. Transport 30 (2), 152–161. http://dx.doi.org/10.3846/16484142.2015.1046137.

Daganzo, C., 2007. Urban gridlock: Macroscopic modeling and mitigation approaches. Transp. Res. B 41, 49–62. http://dx.doi.org/10.1016/j.trb.2006.03.001.

Dandl, F., Engelhardt, R., Hyland, M., Tilg, G., Bogenberger, K., Mahmassani, H.S., 2021. Regulating mobility-on-demand services: Tri-level model and Bayesian optimization solution approach. Transp. Res. C 125, 32. http://dx.doi.org/10.1016/j.trc.2021.103075.

Dandl, F., Tilg, G., Rostami-Shahrbabaki, M., Bogenberger, K., 2020. Network fundamental diagram based routing of vehicle fleets in dynamic traffic simulations. In: 2020 IEEE 23rd International Conference on Intelligent Transportation Systems (ITSC). IEEE, pp. 1–8. http://dx.doi.org/10.1109/ITSC45102.2020.9294204.

Elbery, A., Rakha, H., 2019. City-wide eco-routing navigation considering vehicular communication impacts. Sensors 19, 290. http://dx.doi.org/10.3390/s19020290.

Environmental protection agency (EPA), 2003. User's guide to MOBILE, mobile source emission factor model.

EPA, 2010. Motor vehicle emission simulator (MOVES): User guide for MOVES2010b. Technical report. United States environmental protection agency. URL: https://www.nrc.gov/docs/ML1127/ML112720505.pdf.

Fontes, T., Pereira, S., Fernandes, P., Bandeira, J., Coelho, M., 2015. How to combine different microsimulation tools to assess the environmental impacts of road traffic? Lessons and directions. Transp. Res. D 34, 293–306. http://dx.doi.org/10.1016/j.trd.2014.11.012.

Frey, H.C., Liu, B., 2013. Development and evaluation of a simplified version of MOVES for coupling with a traffic simulation model. In: Transportation Research Board 91st Annual Meeting of the Transportation Research Board, Washington DC, USA.

Geroliminis, N., Daganzo, C., 2008. Existence of urban-scale macroscopic fundamental diagrams: Some experimental findings. Transp. Res. B 42, 759–770. http://dx.doi.org/10.1016/j.trb.2008.02.002.

Guo, L., Huang, S., Sadek, A.W., 2013. An evaluation of environmental benefits of time-dependent green routing in the greater Buffalo–Niagara region. J. Intell. Transp. Syst. 17, 18–30. http://dx.doi.org/10.1080/15472450.2012.704336.

Hausberger, S., Rexeis, M., Luz, R., Zallinger, M., 2009. Emission factors from the model PHEM for the HBEFA version 3. URL: https://graz.pure.elsevier.com/de/publications/emission-factors-from-the-model-phem-for-the-hbefa-version-3.

He, H., Yang, K., Liang, H., Menendez, M., Guler, S.I., 2019. Providing public transport priority in the perimeter of urban networks: A bimodal strategy. Transp. Res. C 107, 171–192. http://dx.doi.org/10.1016/j.trc.2019.08.004.

Ingole, D., Mariotte, G., Leclercq, L., 2020. Perimeter gating control and citywide dynamic user equilibrium: A macroscopic modeling framework. Transp. Res. C 111, 22–49. http://dx.doi.org/10.1016/j.trc.2019.11.016.

INRIX, 2016. Europe's traffic hotspots, measuring the impact of congestion in Europe.

Jamshidnejad, A., Papamichail, I., Papageorgiou, M., De Schutter, B., 2017. A mesoscopic integrated urban traffic flow-emission model. Transp. Res. C 75, 45–83. http://dx.doi.org/10.1016/j.trc.2016.11.024.

Jie, L., Van Zuylen, H., Chen, Y., Viti, F., Wilmink, I., 2013. Calibration of a microscopic simulation model for emission calculation. Transp. Res. C 31, 172–184. http://dx.doi.org/10.1016/j.trc.2012.04.008.

Kim, S., Menendez, M., Yeo, H., 2021. Methodology to increase flexibility in inter-region flow control for urban traffic. Transp. Res. Rec. http://dx.doi.org/10.1177/0361198121997424.

Kim, S., Yeo, H., 2017. Evaluating link criticality of road network based on the concept of macroscopic fundamental diagram. Transp. A Transp. Sci. 13 (2), 162–193. http://dx.doi.org/10.1080/23249935.2016.1231231.

Lejri, D., Can, A., Schiper, N., Leclercq, L., 2018. Accounting for traffic speed dynamics when calculating COPERT and PHEM pollutant emissions at the urban scale. Transp. Res. D 63, 588–603. http://dx.doi.org/10.1016/j.trd.2018.06.023.

Lejri, D., Leclercq, L., 2020. Are average speed emission functions scale-free? Atmos. Environ. 224, 117324. http://dx.doi.org/10.1016/j.atmosenv.2020.117324.

Liu, Y.-H., Ma, J.-L., Li, L., Lin, X.-F., Xu, W.-J., Ding, H., 2018. A high temporal-spatial vehicle emission inventory based on detailed hourly traffic data in a medium-sized city of China. Environ. Pollut. 236, 324–333. http://dx.doi.org/10.1016/j.envpol.2018.01.068.

Loder, A., Bliemer, M.C., Axhausen, K.W., 2022. Optimal pricing and investment in a multi-modal city — Introducing a macroscopic network design problem based on the MFD. Transp. Res. A 156, 113–132. http://dx.doi.org/10.1016/j.tra.2021.11.026.

Lopez, P.A., Behrisch, M., Bieker-Walz, L., Erdmann, J., Flötteröd, Y.-P., Hilbrich, R., Lücken, L., Rummel, J., Wagner, P., ner, E.W., 2018. Microscopic traffic simulation using SUMO. In: The 21st IEEE International Conference on Intelligent Transportation Systems. IEEE, http://dx.doi.org/10.1109/ITSC.2018.8569938.

Lopez, C., Leclercq, L., Krishnakumari, P., Chiabaut, N., van Lint, H., 2017. Revealing the day-to-day regularity of urban congestion patterns with 3D speed maps. Sci. Rep. 7, 1–11. http://dx.doi.org/10.1038/s41598-017-14237-8.

Lu, C.-C., Liu, J., Qu, Y., Peeta, S., Rouphail, N.M., Zhou, X., 2016. Eco-system optimal time-dependent flow assignment in a congested network. Transp. Res. B 94, 217–239. http://dx.doi.org/10.1016/j.trb.2016.09.015.

Luz, R., Hausberger, S., 2013. User guide for the model PHEM, version 11.2. URL: https://graz.pure.elsevier.com/en/publications/user-guide-for-the-model-phem.

Madireddy, M., De Coensel, B., Can, A., Degraeuwe, B., Beusen, B., De Vlieger, I., Botteldooren, D., 2011. Assessment of the impact of speed limit reduction and traffic signal coordination on vehicle emissions using an integrated approach. Transp. Res. D 16 (7), 504–508. http://dx.doi.org/10.1016/j.trd.2011.06.001.

Mariotte, G., Leclercq, L., 2019. Flow exchanges in multi-reservoir systems with spillbacks. Transp. Res. B 122, 327–349. http://dx.doi.org/10.1016/j.trb.2019.02.014.

Mariotte, G., Leclercq, L., Batista, S., Krug, J., Paipuri, M., 2020. Calibration and validation of multi-reservoir MFD models: A case study in lyon. Transp. Res. B 136, 62–86. http://dx.doi.org/10.1016/j.trb.2020.03.006.

Mariotte, G., Leclercq, L., Laval, J.A., 2017. Macroscopic urban dynamics: Analytical and numerical comparisons of existing models. Transp. Res. B 101, 245–267. http://dx.doi.org/10.1016/j.trb.2017.04.002.

Masson-Delmotte, V., Zhai, P., Pörtner, H.-O., Roberts, D., Skea, J., Shukla, P.R., Pirani, A., Moufouma-Okia, W., Péan, C., Pidcock, R., Connors, S., Matthews, J.B.R., Chen, Y., Zhou, X., Gomis, M.I., Lonnoy, E., Maycock, T., Tignor, M., Waterfield, T., 2019. Global warming of 1.5 °C. An IPCC special report on the impacts of global warming of 1.5 °C above pre-industrial levels and related global greenhouse gas emission pathways, in the context of strengthening the global response to the threat of climate change, sustainable development, and efforts to eradicate poverty. URL: https://www.ipcc.ch/site/assets/uploads/sites/2/2019/06/SR15_Full_Report_High_Res.pdf.

Mühlich, N., Gayah, V.V., Menendez, M., 2015. Use of microsimulation for examination of macroscopic fundamental diagram hysteresis patterns for hierarchical urban street networks. Transp. Res. Rec. 2491 (1), 117–126. http://dx.doi.org/10.3141/2491-13.

Ntziachristos, L., Gkatzoflias, D., Kouridis, C., Samaras, Z., 2009. COPERT: A European road transport emission inventory model. In: Information Technologies in Environmental Engineering. Springer Berlin Heidelberg, pp. 491–504.

OpenStreetMap contributors, 2020. Innsbruck dump retrieved from . https://planet.osm.org.

Paipuri, M., Leclercq, L., 2020. Bi-modal macroscopic traffic dynamics in a single region. Transp. Res. B 133, 257–290. http://dx.doi.org/10.1016/j.trb.2020.01.007.

Paipuri, M., Leclercq, L., Krug, J., 2019. Validation of macroscopic fundamental diagrams-based models with microscopic simulations on real networks: Importance of production hysteresis and trip lengths estimation. Transp. Res. Rec. 2673 (5), 478–492. http://dx.doi.org/10.1177/0361198119839340.

Panis, L.I., Broekx, S., Liu, R., 2006. Modelling instantaneous traffic emission and the influence of traffic speed limits. Sci. Total Environ. 371 (1), 270–285. http://dx.doi.org/10.1016/j.scitotenv.2006.08.017.

Pasquale, C., Sacone, S., Siri, S., De Schutter, B., 2017. A multi-class model-based control scheme for reducing congestion and emissions in freeway networks by combining ramp metering and route guidance. Transp. Res. C 80, 384–408. http://dx.doi.org/10.1016/j.trc.2017.04.007.

Quaassdorff, C., Borge, R., Pérez, J., Lumbreras, J., de la Paz, D., de Andrés, J.M., 2016. Microscale traffic simulation and emission estimation in a heavily trafficked roundabout in madrid (Spain). Sci. Total Environ. 566–567, 416–427. http://dx.doi.org/10.1016/j.scitotenv.2016.05.051.

Qurashi, M., Ma, T., Chaniotakis, E., Antoniou, C., 2020. Pc–SPSA: Employing dimensionality reduction to limit SPSA search noise in DTA model calibration. IEEE Trans. Intell. Transp. Syst. 21 (4), 1635–1645. http://dx.doi.org/10.1109/TITS.2019.2915273.

Rakha, H., Ahn, K., Trani, A., 2004. Development of VT-micro model for estimating hot stabilized light duty vehicle and truck emissions. Transp. Res. D 9 (1), 49–74. http://dx.doi.org/10.1016/S1361-9209(03)00054-3.

Ren, Y., Hou, Z., Sirmatel, I.I., Geroliminis, N., 2020. Data driven model free adaptive iterative learning perimeter control for large-scale urban road networks. Transp. Res. C 115, 102618. http://dx.doi.org/10.1016/j.trc.2020.102618.

Saedi, R., Verma, R., Zockaie, A., Ghamami, M., Gates, T.J., 2020. Comparison of support vector and non-linear regression models for estimating large-scale vehicular emissions, incorporating network-wide fundamental diagram for heterogeneous vehicles. Transp. Res. Rec. 2674 (5), 70–84. http://dx.doi.org/10.1177/0361198120914304.

Samaras, C., Tsokolis, D., Toffolo, S., Magra, G., Ntziachristos, L., Samaras, Z., 2019. Enhancing average speed emission models to account for congestion impacts in traffic network link-based simulations. Transp. Res. D 75, 197–210. http://dx.doi.org/10.1016/j.trd.2019.08.029.

Seppecher, M., Leclercq, L., Furno, A., Lejri, D., Vieira da Rocha, T., 2021. Estimation of urban zonal speed dynamics from user-activity-dependent positioning data and regional paths. Transp. Res. C 129, 103183. http://dx.doi.org/10.1016/j.trc.2021.103183.

Shabihkhani, R., Gonzales, J., 2014. Macroscopic relationship between network-wide traffic emissions and fundamental properties of the network. In: Transportation Research Circular E-C197, Symposium Celebrating 50 Years of Traffic Flow Theory Portland, Oregon, USA. pp. 1–15, URL: http://tft.eng.usf.edu/tft50/tft50_papers/P31_Shabihkhani.pdf.

Sirmatel, I.I., Geroliminis, N., 2019. Nonlinear moving horizon estimation for large-scale urban road networks. IEEE Trans. Intell. Transp. Syst. 1–12.

Sun, J., Liu, H.X., 2015. Stochastic eco-routing in a signalized traffic network. Transp. Res. C 59, 32–47. http://dx.doi.org/10.1016/j.trc.2015.06.002, Special Issue on International Symposium on Transportation and Traffic Theory.

Tilg, G., Ul Abedin, Z., Amini, S., Busch, F., 2020. Simulation-based design of urban bi-modal transport systems. Front. Future Transp. 1, http://dx.doi.org/10.3389/ffutr.2020.581622.

TomTom, 2019. European congestion index. URL: https://www.tomtom.com/en_gb/traffic-index/.

Vickrey, W., 2020. Congestion in midtown manhattan in relation to marginal cost pricing. Econ. Transp. 21, 100152. http://dx.doi.org/10.1016/j.ecotra.2019.100152.

Yang, H., Ke, J., Ye, J., 2018b. A universal distribution law of network detour ratios. Transp. Res. C 96, 22–37. http://dx.doi.org/10.1016/j.trc.2018.09.012.

Yang, K., Menendez, M., Zheng, N., 2019. Heterogeneity aware urban traffic control in a connected vehicle environment: A joint framework for congestion pricing and perimeter control. Transp. Res. C 105, 439–455. http://dx.doi.org/10.1016/j.trc.2019.06.007.

Yildirimoglu, M., Geroliminis, N., 2014. Approximating dynamic equilibrium conditions with macroscopic fundamental diagrams. Transp. Res. B 70, 186–200. http://dx.doi.org/10.1016/j.trb.2014.09.002.

Zegeye, S., De Schutter, B., Hellendoorn, J., Breunesse, E., Hegyi, A., 2013. Integrated macroscopic traffic flow, emission, and fuel consumption model for control purposes. Transp. Res. C 31, 158–171. http://dx.doi.org/10.1016/j.trc.2013.01.002.

Zhou, X., Tanvir, S., Lei, H., Taylor, J., Liu, B., Rouphail, N.M., Christopher Frey, H., 2015. Integrating a simplified emission estimation model and mesoscopic dynamic traffic simulator to efficiently evaluate emission impacts of traffic management strategies. Transp. Res. D 37, 123–136. http://dx.doi.org/10.1016/j.trd.2015.04.013.

Zhu, S., Levinson, D., 2015. Do people use the shortest path? An empirical test of wardrop's first principle. PLoS One (10), 1–18. http://dx.doi.org/10.1371/journal.pone.0134322.